



BIROn - Birkbeck Institutional Research Online

Ross, A.J. and Downes, Hilary and Herrin, J.S. and Mittlefehldt, D.W. and Humayun, M. and Smith, C. (2019) The origin of iron silicides in ureilite meteorites. *Geochemistry*, ISSN 0009-2819. (In Press)

Downloaded from: <https://eprints.bbk.ac.uk/id/eprint/29458/>

Usage Guidelines:

Please refer to usage guidelines at <https://eprints.bbk.ac.uk/policies.html>
contact lib-eprints@bbk.ac.uk.

or alternatively

The origin of iron silicides in ureilite meteorites

Aidan J. Ross^{1,2}, Hilary Downes^{1,2,3,4*}, Jason S. Herrin^{5†}

David W. Mittlefehldt⁶, Munir Humayun⁷, Caroline Smith²

¹UCL/Birkbeck Centre for Planetary Sciences, University College London, Gower St, London, WC1E 6BT, UK

²Dept. of Earth Sciences, Natural History Museum, Cromwell Rd, London, SW7 5BD, UK

³Dept. of Earth and Planetary Sciences, Birkbeck University of London, Malet St., London, WC1E 7HX, UK

⁴Lunar and Planetary Institute/USRA, 3600 Bay Area Blvd, Houston, TX 77058, USA

⁵ Earth Observatory of Singapore & Facility for Analysis, Characterisation, Testing, and Simulation, Nanyang Technological University, Singapore 639798

⁶Astromaterials Research Office, NASA Johnson Space Center, 2101 NASA Parkway, Houston, TX 77058, USA

⁷Department of Earth, Ocean and Atmospheric Science & National High Magnetic Field Laboratory, Florida State University, 1800 E. Paul Dirac Drive, Tallahassee, FL 32310, USA

†Previously at: ESC Astromaterials Research Group, Johnson Space Center, 2101 NASA Parkway, Houston, TX 77058, USA

*Corresponding Author.

3 Tables

11 Figures

Version of 12 September 2019

Keywords: Ureilites, Achondrites, Meteorites, Silicides, Metals

57
58
59 **ABSTRACT**
60

61 Ureilite meteorites contain iron silicide minerals including suessite (Fe,Ni)₃Si, hapkeite (Fe₂Si) and
62 xifengite (Fe₅Si₃). Despite occurring mostly in brecciated varieties presumed to be derived from the regolith
63 of the ureilite parent asteroid, suessite has also been confirmed in one lithology of a dimict ureilite (NWA
64 1241). In contrast, Si-bearing Fe-metals occur in both brecciated and unbrecciated ureilites, implying that
65 they were formed throughout the ureilite parent asteroid. We examined major, minor and trace element data
66 of Fe-metals in seven brecciated ureilites (DaG 319, DaG 999, DaG 1000, DaG 1023, DaG 1047, EET
67 83309, and EET 87720) in addition to the dimict ureilite NWA 1241.
68
69

70
71
72 In this study we show that the silicides and Si-bearing metals in ureilites have similar siderophile trace
73 element patterns; therefore, the precursors to the silicides were indigenous to the ureilite parent body. Si-
74 free kamacite grains in brecciated ureilites show flatter, more chondritic siderophile element patterns. They
75 may also be derived from the interior of the ureilite parent body, but some may be of exogenous origin
76 (impactor debris), as are rare taenite grains.
77
78

79
80 On Earth, iron silicides are often formed under high-temperature and strongly reducing conditions (e.g.
81 blast furnaces, lightning strikes). On the Moon, hapkeite (Fe₂Si) and other silicides have been found in the
82 regolith where they were formed by impact-induced space weathering. In the Stardust aerogel, iron silicides
83 derived from comet Wild2 were also formed by an impact-related reduction process. Silicides in ureilite
84 regolith breccias may have formed by similar processes but ureilites additionally contain abundant
85 elemental carbon which probably acted as a reducing agent, thus larger and more abundant silicide grains
86 were formed than in the lunar regolith or cometary material. The origin of suessite in NWA 1241 may be
87 analogous to that of reduced lithologies in the terrestrial mantle, although a regolith origin may also be
88 possible since this sample is shown here to be a dimict breccia.
89
90
91
92
93
94
95
96

97 **1. INTRODUCTION**
98

99 In 1982, Keil et al. discovered the first naturally occurring iron silicide in the brecciated ureilite meteorite
100 North Haig. Ureilite meteorites are carbon-bearing ultramafic achondrites, most of which are unbrecciated
101 and thought to represent samples of an asteroidal mantle (e.g. Scott et al., 1993; Goodrich et al., 2004).
102 Their major and bulk trace element compositions are consistent with a restitic origin from a differentiated
103 asteroid after loss of basaltic and metallic melts (e.g. Warren & Kallemeyn 1992; Mittlefehldt et al., 1998;
104 Singletary & Grove 2003; 2006; Kita et al., 2004; Rankenburg et al., 2008). Some ureilites are polymict
105 fragmental breccias consisting of welded lithic clasts and isolated mineral fragments (Jacques and
106
107
108

113
114
115 Fitzgerald, 1982; Prinz et al., 1987; Goodrich et al., 2004; Downes et al., 2008). Most clasts consist of
116 typical ureilitic material but other materials are also found, including clasts similar to R- and E-chondrite
117 types (Downes et al., 2008) and ureilitic melt rocks (Cohen et al., 2004). Solar wind implanted gases in
118 some brecciated ureilites confirm a regolith origin (Ott et al., 1990, 1993, Rai et al., 2003).
119
120
121

122 The formation of ureilites is still a controversial and unsettled problem in meteoritics (e.g., Goodrich et al.,
123 2007; 2013a; Warren, 2012). Nevertheless, the history of ureilite meteorites can be divided into two main
124 stages (Warren and Kallemeyn 1989; Downes et al., 2008; Herrin et al., 2010). The original ureilite parent
125 body had a range of initial silicate compositions (e.g., Warren, 2012) and experienced extensive partial
126 melting of the metal-sulfide and silicate systems. Results from short-lived isotopic chronometers indicate
127 that this differentiation occurred within ~1 Myr of formation of CAIs in the solar nebula (van Kooten et al.,
128 2017). While it was still hot, the ureilite parent body experienced profound mechanical disruption by a large
129 impact (Warren and Kallemeyn 1989; Herrin et al., 2010). Lithic fragments from disrupted portions of the
130 ureilite parent body then reassembled to form a macroscopically brecciated daughter body around which a
131 regolith formed and from which all ureilite meteorites appear to be derived. The Almahata Sitta meteorites
132 derived from the fall of ~4 m diameter asteroid 2008 TC₃ in Sudan (Jenniskens et al., 2009) show that O-,
133 E- and C chondrite fragments are common within the portion of the ureilite-dominated polymict breccia
134 represented by this bolide (Goodrich et al., 2015).
135
136
137
138
139
140
141

142 Naturally occurring iron silicide minerals, first described and named by Keil et al. (1982), have been
143 reported from many brecciated (polymict) ureilite meteorites (Mittlefehldt et al., 2007; Herrin et al., 2008;
144 Smith et al., 2008; 2010; Ross et al., 2010), and from NWA 1241, originally described as being unbrecciated
145 (Ikeda 2007). In contrast, Si-bearing metals occur in both brecciated and unbrecciated ureilites (Goodrich
146 et al., 2013b), although some of them may be exogenic (Boleaga and Goodrich, 2019). We have investigated
147 the nature, composition and origin of iron silicides and Si-bearing metals in several ureilites, in an attempt
148 to determine their mode of formation. Possibilities include that they could represent fragments of the core
149 of the ureilite parent body (Ross et al., 2009), could have formed from reduction of silicate minerals in the
150 mantle of the parent body (Keil et al., 1982), or formed by space weathering processes in the regolith similar
151 to those which occur on the Moon (Anand et al., 2004).
152
153
154
155
156

157 We examined the petrography, major, minor and trace element chemistry of metal phases in eight ureilite
158 samples: Dar al Gani (DaG) 319, DaG 999, DaG 1000, DaG 1023, DaG 1047, Elephant Moraine (EET)
159 83309, EET 87720, and northwest Africa (NWA) 1241. The first seven are brecciated ureilites, while NWA
160 1241 had previously been described as unbrecciated (Ikeda 2007) but we find it to be dimict. Most of these
161 samples are well characterised for their silicate mineralogy (Downes et al., 2008). The EET samples are
162
163
164
165
166
167
168

169
170
171 known to be regolith-derived from studies of their noble gases (Ott et al., 1991, 1993). Some of the DaG
172 might be paired, but this is difficult to determine for polymict breccias (cf., Goodrich et al., 2004).
173
174
175
176
177
178

179 **2. BACKGROUND TO IRON SILICIDES AND SI-BEARING METALS**

182 Fig. 1 shows the compositions of named iron silicide minerals as defined by the International Mineralogical
183 Association (IMA). Keil et al. (1982) first described suessite from polymict ureilites and proposed that it
184 formed within the ureilite mantle from reduction of silicates. Further ureilite silicides not analysed in this
185 paper include hapkeite (Fe_2Si) in a section of dimict ureilite FRO 90228 reported by Smith (2008), and the
186 presence of suessite, hapkeite and naquite in polymict ureilite DaG 1066 reported by Moggi Cecchi et al.
187 (2015). Potentially extra-terrestrial iron silicides reported from cosmic dusts from the Yanshan mountains
188 contain xifengite (Fe_3Si_3) and gupeiite (Fe_3Si) (Yu 1984), and deposits at the Younger Dryas boundary
189 contain suessite ($(\text{Fe,Ni})_3\text{Si}$) (Wu et al., 2013). Hapkeite is also an extremely rare phase in lunar regolith
190 material (Anand et al., 2004) which may have an impact-induced vapor deposition origin. Other iron
191 silicides, including FeSi and FeSi_2 , have been found in lunar meteorite Dhofar 280 (Anand et al., 2004;
192 Nazarov et al., 2012). Suttle and Genge (2017) found suessite in micrometeorites from Late Cretaceous
193 chalks from the United Kingdom. Various iron silicides were found by Reitmeijer et al. (2008) in impact-
194 produced aerogel tracks in samples from comet Wild2. Other extraterrestrial silicides such as perryite
195 ($(\text{Ni,Fe})_8(\text{Si,P})_3$) occur in the Horse Creek ungrouped iron meteorite (Buchwald 1975) and enstatite
196 chondrites (Wasson and Wai 1970), whereas brownleeite (MnSi) is known from interplanetary dust
197 (Nakamura-Messenger et al., 2010). Ni-rich silicides have recently been discovered in aubrite meteorites
198 (Garvie et al., 2018). Silicides have not yet been reported from enstatite chondrite meteorites.
199
200
201
202
203
204
205
206

207 The Earth's mantle provides some rare examples of iron silicides. Several IMA-approved iron silicide
208 minerals were originally found and described from the Luobusha ophiolite complex in Tibet (Fig. 1) where
209 podiform mantle chromitites have yielded luobusaite ($\text{Fe}_{0.84}\text{Si}_2$; Bai et al., 2006), naquite (formerly known
210 as fersilicite; FeSi; Shi et al., 2012) and linzhiite (formerly known as ferdasilicite; FeSi_2 ; Li et al., 2012).
211 However, Ballhaus et al (2017) have suggested that these phases may have formed via lightning strikes on
212 surface outcrops. Ishimaru et al. (2009) described iron-titanium silicides in mantle peridotite xenoliths from
213 beneath Kamchatka (Russia), whereas Pankov and Spetsius (1989) and Shiryaev et al. (2008) reported the
214 presence of FeSi_2 in mantle-derived kimberlites in Russia. Griffin et al. (2016) described Fe_3Si from mantle-
215 derived materials in Late Cretaceous ash deposits on Mount Carmel in Israel, although a recent paper argues
216
217
218
219
220
221
222
223
224

225
226
227 that these and other mantle-derived super-reduced phases including the silicides may be caused by
228 contamination during sample preparation (Litasov et al., 2019). Mavlyanovite (Mn_5Si_3), the manganese
229 analogue of xifengite, has also been reported from a lamproite in Uzbekistan (Yusupov et al., 2009).
230
231

232 Fulgurites (rocks formed when lightning is discharged into the ground) are another source of naturally-
233 occurring terrestrial iron silicides (e.g. Essene and Fisher 1986; Parnell et al., 2008). Pasek et al. (2012)
234 reported the presence of Fe_3Si , Fe_2Si and Fe_5Si_3 (and possibly Fe_8Si_3 and Fe_7Si_3) in fulgurites from
235 Pennsylvania. Silicides formed in fulgurites have experienced high temperatures and very low
236 (atmospheric) pressures over a very short time span (e.g., Pasek and Pasek, 2018). Ballhaus et al (2017)
237 produced xifengite in experiments in which basalt was exposed to artificial lightning strikes which formed
238 high-temperature plasmas in the presence of graphite.
239
240
241
242

243 Artificial iron silicides are also formed at high temperatures and low pressures in industrial processes such
244 as coke-making (Ye et al., 2013) and steel production (Viswanathan et al., 2009). Fig. 2 is part of a
245 metallurgical phase diagram of the Ni-free Fe-Si at 1 atm pressure (Yuan et al., 2007), showing that the
246 stable phases under these conditions are Fe_3Si (gupeite), Fe_5Si_3 (xifengite) and $FeSi$ (naquite).
247
248
249

250 Metals with up to 4 wt% Si occur in enstatite chondrite meteorites (Zhang et al., 1995) and up to 2.4 wt%
251 Si in aubrites (Garvie et al., 2018). Lauretta et al. (2001) reported that metal in Type I chondrules contained
252 up to 3.2 wt% Si. Fe,Ni metals in unbrecciated ureilites contain a maximum of 5 wt% Si (Goodrich et al.,
253 2013b; Horstmann et al., 2014a). This leads to several questions concerning the relationship between the
254 silicides in the asteroidal regolith and the indigenous Si-bearing metals in the asteroidal interior and whether
255 conditions in the regolith environment might have favored iron silicide production.
256
257
258
259
260
261

262 **3. ANALYTICAL METHODS**

263
264 All samples were prepared or provided as polished sections. Initial examination was conducted, using
265 petrographic microscopy and a scanning electron microscope (SEM). The SEM was used to obtain
266 backscattered electron (BSE) images and for semi-quantitative energy dispersive spectroscopy to get an
267 overview of sample textures, location of metallic minerals, and levels of oxidation caused by weathering.
268 This information was used in preparation for analysis using the electron microprobe (EMPA) and laser-
269 ablation inductively coupled plasma mass spectrometry (LA-ICP-MS) as described below.
270
271
272
273
274
275
276
277
278
279
280

281
282
283 Petrographic investigations of EET 83309, EET 87720, DaG 319 and DaG 1047 were conducted on the
284 JEOL 5900LV and LEO 1455VP SEMs at the Natural History Museum, London, with an accelerating
285 voltage of either 15 kV or 20 kV and a beam current of ~2 nA.
286
287

288 All quantitative major and minor element analyses were done by electron microprobes using wavelength-
289 dispersive spectroscopy. Compositions of metal and silicide phases in most samples were initially
290 characterized at NASA Johnson Space Center on a Cameca SX100 microprobe. Typical operating
291 parameters were a 20 kV accelerating voltage and a beam current of 40 nA. Standards for calibration were
292 a combination of natural and synthetic minerals and metals. For larger grains, multiple analyses were
293 performed to discern any compositional heterogeneity. Later analyses on silicides in NWA 1241 were
294 performed using NASA's JEOL JXA 8530-F Field Emission electron microprobe. These analyses were
295 done with an accelerating voltage of 15 kV, a 40 nA beam current, and the beam in spot mode (~0.3 μm) to
296 achieve a finer resolution analysis volume for zoning profiles. For sample DaG 999 only, additional data
297 on metals and silicides were obtained at Nanyang Technological University. Two new sections were studied
298 using a JEOL JXA 8530-F Field Emission electron microprobe with an accelerating voltage of 15 kV and
299 a 20 nA beam current. For samples DaG 319 and DaG 1047, electron microprobe data were collected on
300 the Cameca SX100 instrument at the Natural History Museum, London, with an accelerating voltage of 20
301 kV and a beam current of 20 nA. Results are presented in Tables 1 (metals) and 2 (silicides).
302
303

304 Trace element concentrations for DaG 1000, EET 83309, EET 87720, and NWA1241 were determined at
305 the Plasma Analytical Facility of the National High Magnetic Field Laboratory at Florida State University.
306 Measurements were performed using a New Wave Research UP-213 (Nd:YAG 213 nm) laser ablation
307 system coupled to a Finnigan Element™ magnetic sector ICP-MS. All analyses were performed using a
308 laser repetition rate of 10 Hz and at 50% power output. Further information about the instrumentation setup
309 used in this study, including typical relative sensitivity factors for analysis of metals, are detailed in
310 Humayun et al. (2007). All data was acquired in low resolution mode ($m/\Delta m = 300$). Overall spot sizes
311 varied from 30 to 150 μm , with most analyses performed at 30-40 μm . Because of the small grain sizes,
312 certain elements (e.g. W, Mo) were below detection limit in many analyses and are not considered in our
313 discussion. External calibration standards used were the IVB iron meteorite Hoba, the IIA iron meteorite
314 North Chile (Filomena) and NIST SRM 1263a steel, chosen because of their well-determined element
315 compositions from multiple analyses (Campbell and Humayun 1998; Campbell and Humayun 1999;
316 Campbell et al., 2002; Wasson et al., 1989). Blank-corrected intensities were converted to elemental
317 abundances by normalization to Ni content determined by previous EMP analyses. Analytical precision for
318 most elements was <10% based on repeat measurements of calibration standards.
319
320
321
322
323
324
325
326
327
328
329
330
331

337
338
339 For DaG 319 and DaG 1047, trace elements were analyzed by LA-ICP-MS at NASA JSC using a New
340 Wave UP-193 solid state laser ablation system attached to a Thermo Scientific Element XR™ magnetic
341 sector ICP-MS in low resolution mode ($m/\Delta m = 300$). Laser power was 1-2 GW/cm², with a repetition rate
342 of 10 Hz. Spot sizes varied from 20 to 100 μm, depending on metal/silicide grain size. External calibration
343 standards used were the IVB iron meteorite Hoba, the IIA iron meteorite North Chile (Filomena), and NIST
344 SRM 1168 and NIST SRM 1178 steels, chosen because of their well-determined element compositions
345 from multiple analyses (Campbell and Humayun 1999; Campbell et al., 2002; Campbell and Humayun
346 2005; Wasson et al. 1989; Wasson et al. 1998). Corrected intensities were converted to elemental
347 abundances by normalization to Ni content determined by previous EMP analyses. Where multiple isotopes
348 were analyzed, a weighted mean was calculated.
349
350
351
352
353
354
355
356

357 **4. PETROGRAPHY**

358
359 Sections of eight meteorites were studied petrographically. These samples can be grouped into three sets:
360 two cold desert samples from the Elephant Moraine area of Antarctica (EET 83309 and EET 87720), five
361 hot desert samples from the Dar al Gani area of Libya (DaG 319, DaG 999, DaG 1000, DaG 1023 and DaG
362 1047), and one hot desert sample from Northwest Africa from a non-specific location in Libya (NWA
363 1241).
364
365
366

367 Seven of the samples have been previously classified as polymict, brecciated ureilites. EET 83309 and
368 EET 87720 are similar in texture (Downes et al., 2008), although they are not paired. EET 83309 (Prinz et
369 al., 1987) consists of angular clasts of ureilitic olivine, pigeonite and rare augite. EET 87720 similarly
370 largely consists of clasts of shocked and unshocked ureilitic silicate minerals, in a brecciated matrix of
371 similar material. Silicate minerals analysed by EMPA in several of the same meteorite sections were
372 reported by Downes et al. (2008), where additional petrographic descriptions of these samples can also be
373 found. All these clasts are within the normal range of silicate minerals from unbrecciated ureilites. Polymict
374 ureilites DaG 319, DaG 999, DaG 1000, DaG 1023 and DaG 1047 have been described as coming from
375 close proximity in the Dar al Gani area (Grossman, 1998; Russell et al., 2003; Connolly et al., 2007) but it
376 is not known if they are actually paired. The DaG samples are similar in texture, containing numerous
377 ureilitic silicate minerals of the range of compositions seen in unbrecciated ureilites, displaying different
378 shock levels, as well as rare clasts of non-ureilitic material (e.g. Ikeda et al., 2000; Kita et al., 2004, Downes
379 et al., 2008). Metals in the clasts of non-ureilitic material in EET 83309, EET 87720 and the DaG samples
380
381
382
383
384
385
386
387
388
389
390
391
392

393
394
395 (Downes et al., 2008; Ross et al, 2010) were excluded from this present study, as they are clearly unrelated
396 to ureilites.
397

398
399 NWA 1241 was described as a monomict ureilite by Ikeda (2007), who stated that it was not brecciated and
400 that it contained suessite. Until that discovery, suessite had only been described from polymict ureilites.
401 We confirm the presence of suessite in this sample but have evidence for a dimict character of NWA 1241
402 (Fig. 3). We purchased a sample of NWA 1241 that consisted of two chips; a larger one that is coarse-
403 grained with minimal evidence for alteration (hereafter, lithology A), and a smaller one that is finer-grained
404 and heavily rusted (lithology B). Petrographic examination of thin-sections made from the two fragments
405 confirmed that they are different lithologies and contain distinct textures and differing silicate compositions.
406 The distinct petrography of NWA 1241-A and NWA 1241-B indicates that the original meteorite was
407 certainly dimict and could have been polymict, contradicting the initial classification as a monomict ureilite
408 based on a single thin section (Ikeda, 2007). Dimict ureilite meteorites consisting of two contrasting
409 fragments of ureilites with different textures and mineral chemistry have previously been reported from the
410 Frontier Mountains (FRO) area of the Antarctic by Smith et al (2000).
411

412
413 Based on mineral compositions and textures, lithology B is equivalent to the section described by Ikeda
414 (2007). The texture of lithology B is difficult to ascertain because metallic phases in the chip are highly
415 oxidized, which caused substantial expansion of intergranular boundaries, extensive dark staining
416 (optical)/brightness (backscattered electrons), and facilitated substantial grain plucking (Fig. 3).
417 Furthermore, thick reduced rims on olivine containing minute metal grains make their margins opaque, and
418 these blend into the rusty regions where many of the Fe-silicides reside. Backscattered electron images
419 suggest that lithology B might include intergranular brecciation, but this could be a weathering artifact in
420 which expansion of metallic phases as they oxidized caused fragmentation of silicates. Regardless, lithology
421 B is not a fragmental breccia. We analyzed 11 olivine cores in lithology B and their forsterite contents (Fo)
422 have a narrow range of 82.2-83.0 (Fig. 4). We have analyzed 6 pyroxene cores and most of them have
423 compositions of $Wo_{8.8}En_{76.4}Fs_{14.8}$, but one grain is more magnesian - $Wo_{8.4}En_{80.5}Fs_{11.1}$ (Fig. 4). Our analyses
424 of lithology B phases match those of Ikeda (2007) (Fig. 4). Ikeda (2007) found suessite in his section of
425 NWA 1241, and we have found it only in lithology B. In contrast, lithology A is metal-poor and has the
426 typical ureilite granulitic texture consisting of coarse anhedral olivine and pyroxene grains that meet in
427 triple junctions and have curved intergranular boundaries. Olivine cores in lithology A are uniform in
428 composition with Fo of 89.1 ± 0.1 (Fig. 4). Pyroxene grains are pigeonite, with average core compositions
429 of $Wo_{6.85 \pm 0.02}En_{83.56 \pm 0.04}Fs_{9.59 \pm 0.03}$ (Fig. 4).
430
431
432
433
434
435
436
437
438
439
440
441
442
443

449
450
451 Most of the silicides found in this study were suessite ((Fe,Ni)₃Si). We found xifengite (Fe₅Si₃) only in
452 DaG 999 and EET 87720, and hapkeite was not observed in any of our samples. Iron silicides are observed
453 in three distinct petrographic occurrences in ureilites:
454
455

- 456 a) “Interstitial” coarse suessite found in lithology B of NWA 1241 (Ikeda 2007; Mittlefehldt et al.,
457 2007). This occurrence in the unbrecciated lithology B may allow for definition of the formation
458 mechanism of silicide minerals within ureilites in general. The occurrence described in North Haig
459 (Keil et al., 1982) appears to be similar. Fig. 5 shows examples of coarse in-situ suessite grains in
460 NWA 1241-B. One grain occurs interstitial to four pyroxene grains in textural equilibrium and is
461 texturally similar to grain boundary metal in unbrecciated ureilites (cf., Goodrich et al., 2013b).
462 This homogeneous and abundant population of silicides may be close their site of production.
463
464 b) Fragments on the mm- μ m-scale grains, found in EET 83309, EET 87720, DaG 319, DaG 1000,
465 and DaG 1047 as isolated clasts or adhering to mineral or lithic fragments and are sometimes
466 rounded. One grain in DaG 999 (Fig. 6) consists of two silicides of contrasting compositions, the
467 larger portion being xifengite and the smaller part being suessite. The boundary between the two
468 parts is sharp but not straight. Unfortunately, this grain was discovered too late to be included in
469 the LA-ICP-MS study. Fig. 7 shows examples of silicides in EET 83309 and EET 87720, together
470 with examples of kamacite, all of which have been analyzed by LA-ICP-MS. These silicides
471 coexist with unrelated metals and sulfides (Herrin et al., 2006). This population was probably
472 gardened from their original site of production and re-deposited in regolith breccias by impact.
473
474 c) Grains in “shock-melt veins” as described by Smith et al. (2008) in paired dimict ureilites FRO
475 90168/90228/93008 together with kamacite and iron phosphides. This is a disequilibrium
476 assemblage wherein silicides were either stabilized locally at μ m scales or else transported by
477 shock melts. This observation may be significant in terms of the origin of ureilitic silicides.
478
479
480
481
482
483
484
485
486
487
488

489 **5. COMPOSITIONS OF METALS AND SILICIDES**

491 5.1 EMPA results

492
493 Tables 1 and 2 give major and minor element compositions for representative metal and silicides analyzed
494 in the ureilite samples. Fig. 8 shows the variation in Ni and Si in all the individual analyses in different
495 metal and silicide species, compared with metals in unbrecciated ureilites (Goodrich et al., 2013b;
496 Horstmann et al., 2014a) and slightly greater than the highest amount of Si found in metals in enstatite
497 chondrites (Zhang et al., 1995) and Type I chondrules (Lauretta et al., 2001). We have identified three types
498
499
500

505
506
507 of metal (Table 1): Si-free kamacite, Si-bearing kamacite, and taenite, as well as three types of silicide
508 (Table 2): suessite, xifengite, and a third, non-stoichiometric type that we refer to as “low-Si silicides”. Fig.
509 9a shows these defined phases on a ternary diagram of Fe–Si–Ni+Co and Fig. 9b shows their Ni-Co
510 relationships. Fig. 2 shows a histogram for the number of grains of different Si contents found in this study.
511
512

513
514 We define Si-free kamacite here as containing ≤ 0.1 wt% Si and ≤ 6.91 wt% Ni (the maximum found in Si-
515 free grain boundary metal in unbrecciated ureilites (Goodrich et al., 2013b)). Si-free kamacite is particularly
516 abundant in a single large, mosaicsed ureilitic clast in EET 87720, but also occurs in DaG 1047 and rarely
517 (one grain per section) in samples DaG 319, DaG 1000, EET 83309 and NWA 1241-A. It contains 0.34-
518 6.89 wt% Ni, 0.06-0.61 wt% Co, ≤ 0.33 wt% Cr and ≤ 1.53 wt% P.
519
520

521
522 Si-bearing kamacite grains are defined as those that plot within the field of grain boundary metal from
523 unbrecciated ureilites reported by Goodrich et al. (2013b) and Horstmann et al. (2014a) to have 0.1 to 5.1
524 wt% Si and < 8 wt% Ni (shown in the background of Fig. 8) We found Si-bearing kamacite in samples EET
525 83309, DaG 319, DaG 999, DaG 1000 and DaG 1047. They contain 0.13-4.91 wt% Si, 0.42-7.97 wt% Ni,
526 0.06-0.61 wt% Co, ≤ 1.3 wt% Cr and 0.06-2.38 wt% P. The most Ni-rich of these have Ni contents outside
527 the kamacite field in the Fe-Ni system (Yang et al., 1996), but the stability field for kamacite (α iron)
528 expands to higher Ni contents with increasing Si and P contents (Ackerbauer et al., 2009).
529
530

531
532 Grains of taenite (classified here with Ni > 8 wt%), were found in EET 87720, DaG 999, DaG 1000 and
533 DaG 1047. They show a wide range of Ni (up to 29 wt%) but low Si contents (mostly below detection
534 limit). It is likely that they are derived from chondritic impactors in the same way that some of the silicate
535 minerals in brecciated polymict ureilites are derived (Downes et al., 2008), since taenite has never been
536 reported in grain boundary metal from unbrecciated ureilites. As such, trace element data for these metals
537 are not considered and we do not discuss their origin further.
538
539

540
541 Table 2 reports representative major and minor element compositions of the ureilitic silicides. Fig. 8 shows
542 a detailed inset for the mineral suessite. Found mostly in NWA 1241-B and DaG 1023 but present in all
543 samples except NWA 1241-A, it has a distribution maximum near stoichiometric suessite: $(\text{Fe,Ni})_3\text{Si}$ (Fig.
544 2) but with a range of Ni contents (Fig. 8). Keil et al. (1982) also found a range of compositions that they
545 defined as suessite (outlined in the inset of Fig. 8) with a low-Ni and high-Ni divide at 2.7 wt%. Keil et al.
546 (1982) found that low-Ni suessite dominated their sample, whereas here high-Ni suessite is the dominant
547 phase in almost all samples where suessite is found. The range of Ni values here does not exceed the 6.4
548 wt% found by Keil et al. (1982), we found a maximum of 5.65 wt%, but the minimum Ni was found to be
549 0.08 wt%, lower than the 0.5 wt% found by Keil et al. (1982). Such low Ni content could be considered to
550
551
552
553
554
555
556

561
562
563 be gupeite, although this grain contains more Si than the ideal gupeite. Keil et al. (1982) gave atomic
564 proportions for two averaged suessites: low-Ni suessite $(\text{Fe,Ni,Co,Cr})_{\Sigma=2.84}(\text{Si,P})_{\Sigma=1}$ and high-Ni suessite
565 $(\text{Fe,Ni,Co,Cr})_{\Sigma=3.14}(\text{Si,P})_{\Sigma=1}$. Here we define suessite using atomic proportions with the full range from
566 $(\text{Fe,Ni,Co,Cr})_{\Sigma=2.52}(\text{Si,P})_{\Sigma=1}$ to $(\text{Fe,Ni,Co,Cr})_{\Sigma=3.46}(\text{Si,P})_{\Sigma=1}$. This corresponds to a Si range of 12.48-16.79
567 wt% (expanded from that of Keil et al. (1982) of 12.6-16.4 wt%). The suessite also contains 0.06-0.43 wt%
568 Co, 0.05-1.46 wt% Cr and ≤ 0.64 wt% P.
569
570
571

572
573 Three grains with compositions close to xifengite (Fe_3Si_3) were found, with 1.01-3.91 wt% Ni, 0.1-0.3 wt%
574 Co, 0.89-1.29 wt% Cr and 0.28-0.81 wt% P (Table 2). A microprobe traverse across a DaG 999 grain,
575 which consists of two phases in contact, shows that Ni, Cr and P all increase across the boundary from
576 suessite to xifengite (Fig. 6). Mn was also higher in the xifengite part of the grain than in the suessite (Fig.
577 6b). The Cr content is variable within the xifengite, with distinctly higher values in the center of the grain.
578
579
580

581 An intermediate group with Si contents between the Si-bearing kamacite and suessite has a wide range of
582 non-stoichiometric Si contents (Fig. 2) and we classify these as “low-Si silicides” (Fig. 8 and Fig. 9a).
583 These grains have Si contents between 5.13 and 12.2 wt % and have Ni between 0.07 and 7.6 wt%. These
584 compositions have not been reported by previous studies of ureilite metals or silicides (Keil et al., 1982;
585 Goodrich et al., 2013b; Horstmann et al., 2014a). Minor element concentrations are 0.06-0.47 wt% Co,
586 ≤ 1.11 wt% Cr and ≤ 0.79 wt% P. The apparent continuous range of Si contents between the grain boundary
587 metal compositions of Goodrich et al. (2013b) and the suessite compositions may indicate either very fine-
588 scale mixtures of silicide and metal, or the presence of metal alloys with variable Si contents.
589
590
591
592

593 A strong positive correlation is observed between Co and Ni in the metals and silicides (Fig. 9b). There is
594 no clear distinction between any of the defined metal and silicides groups and our data overlap the range of
595 those from Goodrich et al. (2013b) for grain boundary metals in unbrecciated ureilites. Goodrich et al.
596 (2013b) found a non-chondritic Ni/Co ratio of 13.6 in metals from unbrecciated ureilites. Our data fall close
597 to the same trendline and trendlines through the groups of each metal and silicide type fall close to or on
598 the trendline defined by Goodrich et al. (2013b). The fact that most of the Si-free kamacite data have non-
599 chondritic Ni/Co ratios implies that these minerals were not derived from chondritic impactors but are part
600 of the suite of indigenous ureilitic metals. The lunar hapkeite analysis (Anand et al., 2004) clearly falls
601 away from the ureilitic data, and plots below the chondritic ratio.
602
603
604
605
606

607 5.2 LA-ICP-MS results

608
609 Table 3 contains siderophile trace element data for metal and silicide phases. Results are displayed in Fig.
610 10, normalized to Ni and to chondritic abundances (Lodders, 2003).
611
612

617
618
619 Si-free kamacite was analyzed in two samples: DaG 1047 and EET 87720. The latter have near-chondritic
620 patterns or else are depleted in only the most compatible siderophiles (Fig. 10a). Despite their flat patterns,
621 the Si-free kamacites may still be indigenous to the ureilite parent body, as Goodrich et al. (2013b) found
622 similar flat patterns in metals in the unbrecciated ureilite ALHA 81101, which is also a highly shocked
623 ureilite similar to the lithology where these grains were found. Si-free kamacites in DaG 1047 are individual
624 grains scattered in the sample and not associated with any particular lithology, but all fall within the ranges
625 of the data found in grain boundary metals from unbrecciated ureilites by Goodrich et al. (2013b), given as
626 background data in Fig. 10a. Most of the DaG 1047 Si-free kamacite grains have enrichments in the
627 compatible siderophile elements relative to EET 87720 Si-free kamacite grains, but have very similar
628 incompatible siderophile element contents.
629
630
631
632
633

634
635 Si-bearing kamacite was analyzed in DaG 310, DaG 1000, DaG 1047 and EET 83309, as shown in Fig.
636 10b. All grains plot within the field for grain boundary metal from unbrecciated ureilites, with the exception
637 of lower Ge values for many of the analyses. One grain in DaG 1047 has a close to flat pattern and could
638 have originated from a Si-bearing metal grain from an E-chondrite clast, but still falls within the ureilitic
639 grain boundary field.
640
641

642
643 Siderophile element patterns of silicides are variable between grains (Fig. 10c and 10d). Most are
644 fractionated, with the highly compatible siderophile elements (Re-Pt) enriched relative to incompatible
645 siderophile elements (Pd, Au) in a manner similar to that observed in bulk ureilites (Warren et al., 2006;
646 Rankenburg et al., 2008) and in individual grains of many grain boundary metals in ureilites (Goodrich et
647 al., 2013b). Siderophile trace element patterns in bulk unbrecciated ureilites are highly fractionated as a
648 legacy of extensive extraction of metallic sulfide partial melts (Warren et al., 2006; Rankenburg et al.,
649 2008). The metals in unbrecciated ureilites usually show strong siderophile element fractionation (Goodrich
650 et al., 2013b), and because they host the majority of siderophile elements, it is not surprising that bulk
651 ureilites show this pattern. Ureilitic silicides have this same fractionation pattern. There is no significant
652 difference between the fractionation patterns for suessite and xifengite, or between silicides and the Si-
653 bearing kamacite, nor correlation with the Si content of the grains (Fig. 11a). The most meaningful
654 difference between the silicides and grain boundary metals is the Ga/Ge ratio (Fig. 11b); here $Ga/Ge > 1$ for
655 almost all silicides whereas $Ga/Ge < 1$ for most grain boundary metal in unbrecciated ureilites (Goodrich et
656 al. 2013b).
657
658
659
660
661
662
663
664
665

666 **6. DISCUSSION**

667
668
669
670
671
672

673
674
675
676 In this section, we evaluate the evidence for primary and/or secondary formation of Fe-silicides in
677 ureilites. Three explanations could be proposed for the origin of the silicides:
678

- 679 1) They are exogenic to the ureilite parent body and were incorporated into ureilite regolith breccia
680 samples by impact or were injected into lithologies such as NWA 1241-B;
681
- 682 2) Silicides formed within the ureilite parent body in lithologies such as NWA 1241-B that have
683 since been incorporated into the breccias. This would imply that samples like NWA 1241-B are
684 underrepresented in our collections of unbrecciated ureilites;
685
- 686 3) The silicides formed by a reducing process in the regolith of the ureilite source body and were
687 injected into lithologies such as NWA 1241 as a Fe-Si melt.
688

689
690
691
692 We have demonstrated that regolith breccia ureilites contain a variety of metals and silicides (Figs. 8 and
693 9). We have shown that suessite-bearing NWA 1241 is a dimict breccia (Fig. 3 and 4), contrary to previous
694 work which examined only one thin-section that contained a single lithologic component of the rock (Ikeda,
695 2007). Silicides have not been reported in any other monomict or unbrecciated ureilites and their occurrence
696 thus appears to be restricted to brecciated samples and one lithology of NWA 1241. Because textures in
697 our sample of NWA 1241-B are obscured by terrestrial alteration, we cannot claim that intergranular
698 brecciation is entirely absent. However, Ikeda (2007) stated that the suessite-bearing section of NWA 1241
699 he studied was unbrecciated. Regardless, we have demonstrated that the silicides in NWA 1241-B are in
700 textural equilibrium with the silicates, and not in breccia contact (Fig. 5). Silicides are not in chemical
701 equilibrium with surrounding Fe-silicates and thus appear either to have formed within the regolith (for
702 polymict breccias), or to have been included in ureilites by some physical process such as injection of Fe-
703 Si melts. The texture of NWA 1241-B and siderophile trace element compositions of silicides indicate they
704 are indigenous to the ureilite parent body, and Ikeda (2007) concluded that silicides in polymict ureilites
705 were incorporated into the regolith by admixture of a NWA 1241-like lithology.
706
707

708
709
710
711
712
713
714 The fact that extra-terrestrial Fe-silicides occur mostly in regolith breccia ureilites and are also found in the
715 lunar regolith could imply that some process acting on the surfaces of airless bodies may have been
716 responsible for their formation. The high temperatures (1230-1100°C) and extreme reducing conditions
717 necessary for silicide formation (Ikeda 2007) could not have acted on the ureilite asteroidal regolith for
718 long, as they would have quickly homogenized much of the mineralogical and textural diversity observed.
719 Iron silicides can only be in equilibrium with FeO-bearing ureilite silicates at very low oxygen fugacities,
720 so the process that produced them may have required the presence of carbon which is common in ureilites.
721
722
723

729
730
731 Additional evidence for short-duration, non-equilibrium processing of metal in ureilites is provided by the
732 presence of nucleosynthetic Os isotope heterogeneity, including in DaG 319 (Goderis et al., 2015), one of
733 the samples studied here.
734

735
736 The partial melting which left ureilites as residues involved removal of metal-sulfide and basaltic silicate
737 fractions (Warren and Huber 2006). While ureilites typically contain low abundances of metal and sulfide
738 in comparison to other types of achondrites such as HEDs, concentrations of highly refractory/compatible
739 siderophile elements are sometimes present at greater than chondritic abundances in the bulk rocks
740 (Rankenburg et al., 2008). This observation is consistent with the hypothesis that significant fractions of
741 incompatible material have been removed from the parental asteroid, resulting in passive concentration of
742 the more compatible components. The remaining metallic fraction in a typical ureilite is enriched in
743 elements which are most compatible in the solid phase during metal-sulfide melting relative to incompatible
744 elements (Rankenburg et al., 2008; Goodrich et al., 2013b).
745

746
747 Many of the Si-rich kamacites and silicides from the ureilites studied here have the high
748 compatible/incompatible signature typical of bulk unbrecciated and monomict ureilites. Therefore, their
749 trace element composition was likely inherited from Si-bearing metals formed as restites during melting in
750 the metal-sulfide system within the ureilite parent body. This is consistent with the textural occurrence of
751 suessite, mostly as fragments, but also as coarse interstitial grains in NWA 1241-B. Individual grains tend
752 to be homogeneous in major and trace element but different grains have different compositions within the
753 same sample. The difference in Ga/Ge ratios between the silicides and grain boundary metals (Goodrich et
754 al., 2013b) is plausibly due to the silicides having undergone a more significant level of reduction, since
755 Ga could be reduced from surrounding silicates (Schmitt et al., 1989). The similarity in overall fractionation
756 pattern, in combination with the high T, low-fO₂ conditions required for suessite formation (Ikeda, 2007),
757 indicates that the silicides may have been derived from Si-bearing metals within the ureilite parent body.
758

759
760 The Si-rich kamacites could have been the source of the siderophile elements found in the silicides, but the
761 source of the additional Si in the silicides is not so clear. Hapkeite in the lunar regolith was considered by
762 Anand et al. (2004) to have been formed by either reduction by solar wind or condensation from vapor. If
763 the silicides formed on the ureilite parent asteroid, this combination of high-T and low-P could only be
764 realized in the near-surface of a carbon-rich source during or shortly after impact, and therefore was mainly
765 experienced by regolith material. The observation that iron silicides were formed by impacts onto Stardust
766 aerogel (Rietmeijer et al., 2008) also suggests a very short-duration, high-temperature event.
767

785
786
787 However, suessite grains in NWA 1241-B do not display textural evidence for *in-situ* formation by a very
788 rapid, high-T process. The suessite is interstitial between four pyroxene grains, and the grains are either
789 included within pyroxene or at grain boundaries (Fig. 5). These textures are compatible with suessite having
790 formed in, or been mobilized into, the interstices of the silicate framework. The example grains shown in
791 Fig. 5 are in C-poor areas (C would be black in these images). The pyroxene in Fig. 5a shows very minimal
792 reduction (slightly darker blue color) whereas that in Fig. 5b shows more extensive evidence for reduction,
793 and the olivine has reduced rims (lighter green). However, the metal grains in these reduced rims are barely
794 resolved (micron/sub-micron-sized) while the suessite grains are tens of microns in size. Thus, our results
795 on NWA 1241-B do not support an *in-situ* reduction process for formation of suessite in the presence of
796 FeO-bearing pyroxene and olivine for this case, but rather a more persistent process at greater depth within
797 the fractured crust of the parent body.
798
799

800
801
802
803
804 One scenario that might explain the results on NWA 1241-B and the trace element data on silicides is that
805 the silicides were part of a reduced assemblage that accreted late to the parent body. However, although
806 enstatite chondrites form part of the assemblage of foreign fragments in polymict ureilites (including
807 Almahata Sitta), there are also abundant fragments of much more oxidized material, none of which contain
808 silicides. None of the enstatite chondrite fragments analysed so far contain silicides but many of them
809 contain metal with up to 5.6 wt% Si (Horstmann et al., 2014b). However, their siderophile trace element
810 patterns are chondritic, unlike those found in silicides in ureilites. A second scenario is that silicide in NWA
811 1241-B was formed as part of the high-T process that melted some of the reduced metals. Fractional melting
812 in the metal-sulfide system allowed the early-formed, low-T melts to separate from the ureilitic restites,
813 leaving behind restitic, compatible-siderophile-element-rich metal grains. If, during the melting process,
814 the restite metal had been in equilibrium with a Fe-S-Si liquid, trace elements that are Si-avoiding would
815 tend to concentrate in the low-Si metal, e.g. Ga, Ge, As and Au (Chabot et al., 2010). However, the
816 siderophile element data for ureilitic silicides and grain boundary metal (kamacites) do not show different
817 tendencies to concentrate the Si-avoiding elements defined by Chabot et al. (2010) (Fig. 10), as would be
818 expected for this scenario. From this siderophile element evidence it is inferred that Si likely entered pre-
819 existing metal grains under subsolidus, reducing conditions. The Fe-Si phase diagram (Fig. 2) shows that
820 addition of Si to the system reduces the melting temperature. This suggests that the high-Si contents of
821 compatible-siderophile-element-rich metals in ureilites were engendered by high-T reduction of the silicate
822 phase, and that Si-rich metals were not part of the initial accretion assemblage to the ureilite parent body.
823 However, this scenario does not provide a ready explanation for apparent lack of chemical reaction between
824 Si-rich metal and FeO-bearing silicates, as documented in Fig. 5. Rapid injection of Fe-Si melts during
825
826
827
828
829
830
831
832
833
834
835

841
842
843 impact followed by fast cooling may be one explanation for the silicides in NWA 1241, particularly as this
844 sample is now known to be dimict breccia and hence may have been close to the surface of the parent body.
845
846
847
848

849 **7. CONCLUSIONS**

850
851 A wide variety of metals and Fe-silicides in different petrographic contexts have been analyzed in a suite
852 of polymict breccia ureilites, which probably represent the regolith of their parent body, and in the dimict
853 ureilite NWA 1241. The metals are of three main types: Si-free kamacite which shows a range of Ni
854 contents, Si-bearing kamacite, and taenite. Both Si-free and Si-bearing kamacites occur in unbrecciated
855 ureilite grain boundary metal. Our major, minor and trace siderophile element results on metals closely
856 resemble those reported from unbrecciated ureilites indicating that they were likely indigenous to the
857 ureilite parent body. Taenite, however, has not been found in unbrecciated ureilites, and is therefore
858 probably of impactor origin.
859
860
861
862

863
864 The silicides form three types: abundant suessite with variable Ni contents, rare xifengite, and a group of
865 “low-Si silicide” grains that have Si contents between those of Si-bearing kamacite metals and
866 stoichiometric suessites. In one case (DaG 999) a grain is composed of two distinct silicides (suessite and
867 xifengite) in contact. Siderophile element patterns for the silicides are similar to those for the low-Si
868 silicides and the Si-bearing kamacite, indicating a close relationship.
869
870
871

872 The silicides may have been derived from the Si-bearing kamacite by a process of reduction which occurred
873 mainly in the regolith, similar to the impact-induced space weathering process on the Moon. However,
874 suessite in NWA 1241-B appears to be in textural equilibrium with the ureilite silicates and may either have
875 formed at greater depth within the ureilite parent body or was injected as a metallic melt. This sample has
876 been shown in our study to be dimict and hence part of a breccia, which suggests that it may have been
877 formed quite close to the surface of the parent body.
878
879
880

881 The different occurrences of natural silicides in terrestrial and extraterrestrial environments clearly indicate
882 a variety of different origins. Silicides such as suessite and xifengite were mostly formed in situ on the
883 ureilite parent asteroid perhaps by impacts that produced high T and (in the presence of abundant carbon)
884 low fO_2 . Thus, silicides in polymict ureilites were mostly formed by a short-lived, high temperature process
885 that acted in the near-surface environment of their parent asteroid. This is a very different process from that
886 which formed silicides in the terrestrial mantle, and more closely resembles that which formed Fe-silicides
887 in the lunar regolith. The difference between the lunar and ureilite cases may be the result of the much
888
889
890
891

897
898
899 higher abundances of carbon in the latter. We cannot exclude a deeper origin (e.g. reduction in the asteroid
900 mantle) for the suessite found in NWA 1241.
901
902
903
904

905 **8. ACKNOWLEDGEMENTS**

906
907 We would like to thank the reviewers F. Langenhorst and Anonymous for their comments and suggestions
908 for improving this manuscript, and F. Langenhorst and A. Krot for handling this submission. We thank the
909 ANSMET program and the U.S. Antarctic Meteorite Program for recovery and allocation of the Elephant
910 Moraine ureilites examined as part of this study. This work was supported in part by grants from the NASA
911 Cosmochemistry and Planetary Science Research Programs to DWM and MH. We acknowledge NERC
912 funding for a CASE studentship with the NHM to AJR; and a Leverhulme Trust grant to HD. AJR would
913 like to thank J. Spratt, A. Ball and A. Kearsley for analytical assistance at the NHM. The DaG and NWA
914 1241 samples were purchased from Erich Haiderer.
915
916
917
918
919
920
921

922 **FIGURE CAPTIONS:**

923 Fig. 1. Compositions of iron silicide minerals identified by IMA, including idealized compositions and
924 actual compositions from which idealized compositions were derived. Composition of Earth's core from
925 McDonough (2003)
926

927
928 Fig. 2. Fe-Si binary phase diagram at atmospheric pressure with ideal Fe-silicides phases up to 50 atomic
929 % labelled (modified after Yuan et al., 2007). Histogram: atomic % Si for all grains in this study.
930

931 Fig. 3. Merged element maps and backscattered electron images of NWA 1241 lithologies A and B showing
932 textural differences. Locations of textural details of suessite shown in Figs. 5 and 5b are indicated.
933

934 Fig. 4. Silicate mineral compositions for two lithologies of NWA 1241, compared with average data from
935 Ikeda (2007).
936

937 Fig. 5. Merged element maps and backscattered electron images of examples of suessite in NWA 1241
938 lithology B. Different textural settings are: a. grain-boundary metal between pyroxene grains; b. suessite
939 grains at juncture of olivine and pyroxene grains. Bright yellow areas in both images indicate high-Ni
940 suessite.
941

942 Fig. 6. (a) BSE image and (b) false color Si map of a silicide grain in DaG 999, showing two phases (suessite
943 and xifengite). EPMA data of the traverse indicated by the arrow across the boundary between suessite and
944 xifengite in (a) are plotted in (c) for major elements and (d) for minor elements. Spikes in total weight %
945 in (c) indicate bad data points.
946
947

953
954
955 Fig. 7. BSE images for metals and silicides in EET 83309 and EET 87720. Image (i) shows low-Si silicide
956 from EET 83309; images (ii) and (iii) show suessite grains from EET 83309; image (iv) shows kamacite
957 from EET 87720; image (v) shows xifengite from EET 87720; image (vi) shows kamacite with high Ni
958 content from EET 87720.
959

960
961 Fig. 8. Si vs Ni in silicides and metals from brecciated ureilites from this work. Silicide compositions from
962 Keil et al. (1982) (KK'82), Ikeda (2007), Anand et al. (2004) (MA'04), and ideal IMA compositions for
963 gupeite, hapkeite and xifengite are shown. Also shown as background data are those from literature grain
964 boundary (GB) metals in unbrecciated ureilites from Goodrich et al. (2013b), Horstmann et al. (2014a), and
965 Warren & Rubin (2010). Inset shows entire range of suessite compositions found by Keil et al. (1982). All
966 silicides contain Ni within the range of ureilite grain boundary metal but more Si. Individual data points are
967 plotted by meteorite analyzed.
968

969
970 Fig. 9. (a) Atomic % ternary diagram of Fe-Si-Ni+Co in silicides and metals from this study. Data points
971 are plotted by mineral, as defined in Figure 8. Grey lines represent intervals of 10 atomic %, with the base
972 cut off at 50 atomic % Fe. (b) Plot of Ni vs Co weight % in silicides and metals (excluding taenite). Data
973 for grain boundary metals in unbrecciated ureilites are shown in the background for comparison, as well as
974 their trend (Goodrich et al., 2013b).
975

976
977 Fig. 10. Chondrite-normalized siderophile element abundances for: (a) Si-free kamacite; (b) Si-bearing
978 kamacite; (c) low-Si silicides; (d) suessite and xifengite.
979

980
981 Fig. 11. (a) Ir/Pd vs. Si weight % from EPMA analysis for different mineral types; (b) Ga/Ni vs Ge/Ni for
982 different mineral types.
983

984 TABLE CAPTIONS

985
986 Table 1. Representative major element compositions of metals in brecciated ureilites and NWA 1241-B.
987 bdl = below detection limit; na = not analysed.
988

989
990 Table 2. Representative major element compositions of silicides in brecciated ureilites and NWA 1241-B
991 bdl = below detection limit; na = not analysed.
992

993
994 Table 3. Trace element compositions of silicides and metals in brecciated ureilites and NWA 1241-B. Ni
995 (highlighted) was used for internal calibration. Where multiple spot sizes are given, this means the data
996 was averaged from two analyses on the same grain. Si weight % from EPMA analysis. bdl = below
997 detection limit (with detection limit given in brackets for LA-ICP-MS data).
998

999 REFERENCES

1000
1001 Ackerbauer S., Krendelsberger N., Weitzer F., Hiebl K. and Schuster J. C 2009. The constitution of the
1002 ternary system Fe–Ni–Si. *Intermetallics* 17, 414-420.
1003

- 1009
1010
1011 Anand M, Taylor L A, Nazarov M A, Shu J, Mao H-K and Hemley R J 2004. Space weathering on airless
1012 planetary bodies: clues from the lunar mineral hapkeite. *Proc. Nat. Acad. Sci.*, 101, 6847-6851
1013
- 1014 Bai W, Shi N, Fang Q, Li G, Xiong M, Yang J and Rong H. 2006. Luobusaite, a new mineral. *Acta*
1015 *Geologica Sinica*. 80, 656-659.
1016
- 1017 Ballhaus C, Wirth R, Fonseca R O C, Blanchard H, Pröll W, Bragagni A, Nagel T, Schreiber A, Dittrich S,
1018 Thome V, Hezel D C, Below R and Cieszynski H. 2017. Ultra-high pressure and ultra-reduced minerals in
1019 ophiolites may form by lightning strikes. *Geochemical Perspectives Letters* 5, 42-46.
- 1020 Berkley J. L. and Jones J. H. 1982. Primary igneous carbon in ureilites: Petrological implications.
1021 Proceedings, 13th Lunar and Planetary Science Conference, *Journal of Geophysical Research*
1022 87(supplement): A353-A364.
1023
- 1024 Berkley J. L., Taylor G. J., Keil K., Harlow G., and Prinz M. 1980. The nature and origin of ureilites.
1025 *Geochimica et Cosmochimica Acta* 44:1579-1597.
1026
- 1027 Boleaga Y and Goodrich C A 2019. Xenolithic Fe,Ni metal in polymict ureilite meteorites. 50th LPSC
1028 Abstract # 1622.
- 1029 Buchwald V F 1975. Handbook of iron meteorites. Volume 2, 661-664
1030
- 1031 Campbell A J and Humayun M 1998. Microanalysis of platinum group elements in iron meteorites using
1032 Laser Ablation ICP-MS. 30th LPSC Abstract # 1974
1033
- 1034 Campbell A J and Humayun M 1999. Trace element microanalysis in iron meteorites by Laser Ablation
1035 ICPMS. *Anal. Chem.* 71, 939-946
1036
- 1037 Campbell A J and Humayun M 2005. Compositions of group IVB iron meteorites and their parent melt.
1038 *Geochimica et Cosmochimica Acta* 69, 4733-4744.
1039
- 1040 Campbell A J, Humayun M and Weisberg M K 2002. Siderophile element constraints on the formation of
1041 metal in the metal-rich chondrites Bencubbin, Weatherford, and Gujba. *Geochimica et Cosmochimica Acta*
1042 66, 647-660.
- 1043 Chabot N L, Safko T M and McDonough W F 2010. Effect of silicon on trace element partitioning in iron-
1044 bearing metallic melts. *Meteoritics & Planetary Science* 45, 1243-1257.
1045
- 1046 Cohen B A, Goodrich C A and Keil K 2004 Feldspathic clast populations in polymict ureilites: Stalking the
1047 missing basalts from the ureilite parent body. *Geochimica et Cosmochimica Acta* 68, 4249-4266.
1048
- 1049 Connolly H C, Smith C, Benedix G, Folco L, Richter K, Zipfel J, Yamaguchi A, Chennaoui Aoudjehane
1050 H. 2007. The Meteoritical Bulletin #92. *Meteoritics & Planetary Science* 42, 1647-1694.
1051
- 1052 Downes H, Mittlefehldt D. W., Kita N. T., and Valley J.W. 2008. Evidence from polymict ureilite
1053 meteorites for a disrupted and re-accreted single ureilite parent asteroid gardened by several distinct
1054 impactors. *Geochimica et Cosmochimica Acta* 72:4825-4844.
- 1055 Essene E J and Fisher D C 1986. Lightning strike fusion: extreme reduction and metal-silicate liquid
1056 immiscibility. *Science* 234, 198-193.
1057
- 1058 French B V and Eugster H P 1965. Experimental control of oxygen fugacities by graphite-gas equilibria,
1059 *Journal of Geophysical Research* 70, 1529-1539.
1060

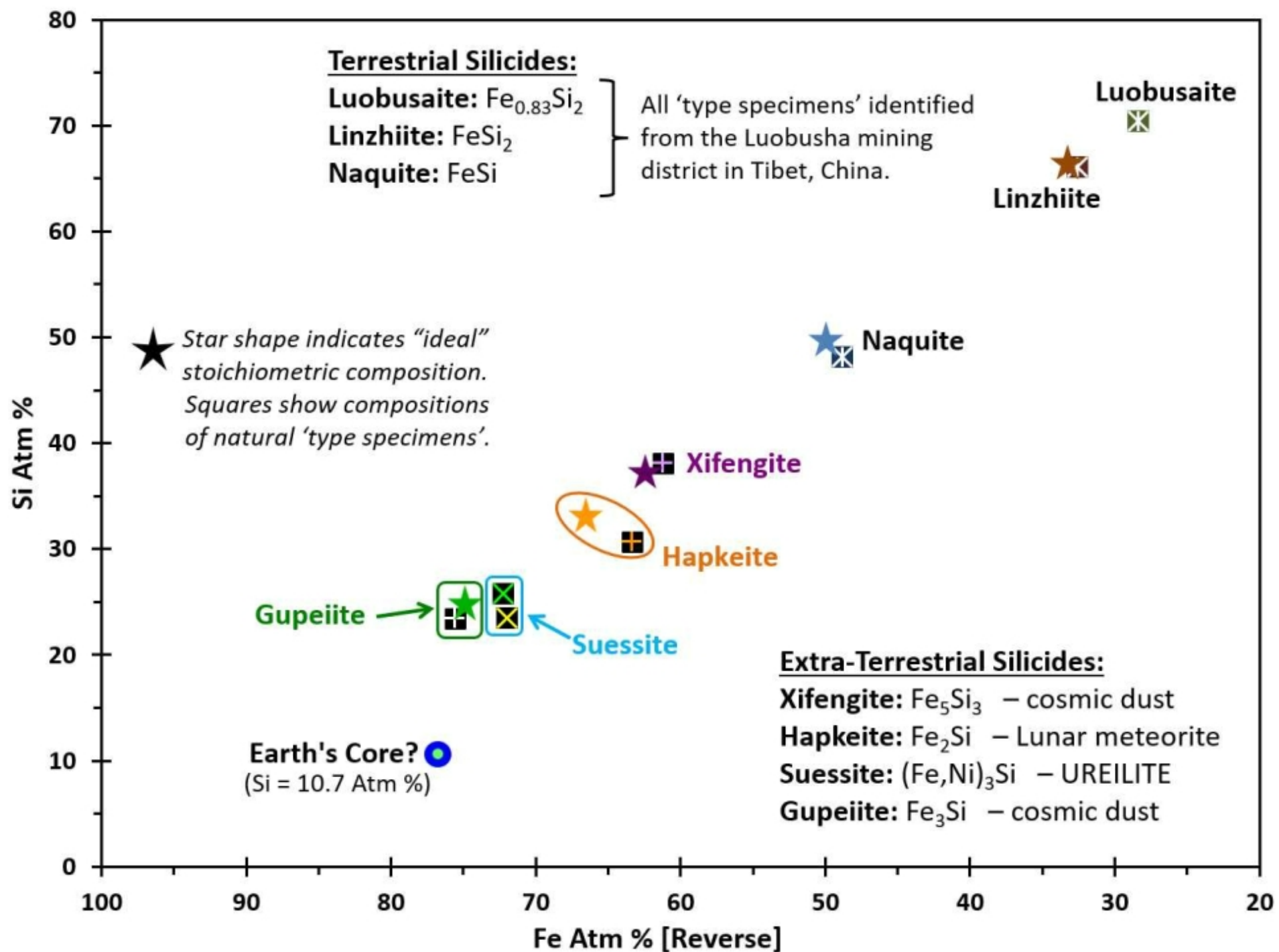
- 1065
1066
1067
1068
1069
1070
1071
1072
1073
1074
1075
1076
1077
1078
1079
1080
1081
1082
1083
1084
1085
1086
1087
1088
1089
1090
1091
1092
1093
1094
1095
1096
1097
1098
1099
1100
1101
1102
1103
1104
1105
1106
1107
1108
1109
1110
1111
1112
1113
1114
1115
1116
1117
1118
1119
1120
- Garvie L A J, Ray S, Wadhwa M, Wittman A and Domanik K 2018. Scrutinising six silicide-bearing samples of metal from the Norton County aubrite. 49th LPSC abstract # 2104.
- Goderis S, Brandon A D, Mayer B and Humayun M 2015. S-process Os isotope enrichment in ureilites by planetary processing. *Earth Planetary Science Letters* 431, 110-118.
- Goodrich C. A. and Berkley J. L. 1986. Primary magmatic carbon in ureilites: Evidence from cohenite-bearing metallic spherules. *Geochimica et Cosmochimica Acta* 50:681-691.
- Goodrich C. A., Scott E. R. D., and Fioretti A. M. 2004. Ureilitic Breccias: Clues to the petrologic structure and impact disruption of the ureilite parent asteroid. *Chemie de Erde* 64: 283-327.
- Goodrich C.A., Van Orman J.A. and Wilson L. 2007. Fractional melting and smelting on the ureilite parent body. *Geochimica et Cosmochimica Acta* 71, 2876-2895.
- Goodrich C.A., Wilson L., Van Orman J.A. and Michel P. 2013a. Comment on “Parent body depth-pressure-temperature relationships and the style of the ureilite anatexis” by P. H. Warren (MAPS 47:209–227). *Meteoritics & Planetary Science* 48, 1096-1106.
- Goodrich C A, Ash R D, Van Orman J A, Domanik K and McDonough W F 2013b. Metallic phases and siderophile elements in main group ureilites: Implications for ureilite petrogenesis. *Geochimica et Cosmochimica Acta* 112, 340-373.
- Goodrich C A, Hartmann W K, O’Brien D P, Weidenschilling S J, Wilson L, Michel P and Jutzi M. 2015. Origin and history of ureilitic material in the solar system: The view from asteroid 2008TC3 and the Almahata Sitta meteorite. *Meteoritics and Planetary Science* 50, 782-809.
- Griffin WL, Gain S E M, Adams D T, Huang J-X, Saunders M, Toledo V, Pearson N J and O’Reilly S Y 2016. First terrestrial occurrence of tistarite (Ti₂O₃): Ultra-low oxygen fugacity in the upper mantle beneath Mount Carmel, Israel. *Geology*, 44, 815-818.
- Grossman J N. 1998. The Meteoritical Bulletin, No. 82, 1998 July. *Meteoritics and Planetary Science* 33, Supplement A221-A239.
- Herrin J S, Mittlefehldt D W, Downes H and Humayun M 2008. Diverse metals and sulfides in polymict ureilites EET 83309 and EET 87720. 38th LPSC abstract # 2404
- Herrin J S, Mittlefehldt D W and Jones J H 2008. Petrogenesis of Fe,Si metals in brecciated ureilites. 71st Annual Meteoritical Society Meeting Abstract # 5327
- Horstmann M, Humayun M, Fisher-Gödde M, Bischoff A and Weybrauch M 2014a. Si-bearing metal and niningerite in Almahata Sitta fine-grained ureilites and insights into the diversity of metal on the ureilite parent body. *Meteoritics and Planetary Science* 49, 1948-1977.
- Horstmann M, Humayun M, and Bischoff A 2014b. Clues to the origin of metal in Almahata Sitta EL and EH chondrites and implications for primitive E chondrite thermal histories. *Geochim. Cosmochim. Acta*. 140, 720-744.
- Humayun M, Simon S B and Grossman L 2007. Tungsten and hafnium microdistribution in calcium-aluminum inclusions (CAIs) from Allende and Efremovka. *Geochim. Cosmochim. Acta* 71, 4609-4627.
- Ikeda Y 2007. Petrology of an unusual ureilite NWA 1241. *Polar Science* 1, 45-53.

- 1121
1122
1123 Ikeda Y, Prinz M, Nehru C. 2000. Lithic and mineral clasts in the Dar al Gani (DaG) 319 polymict ureilite.
1124 *Antarctic Meteorite Research* 13, 177-221.
1125
1126 Ishimaru S, Arai S, and Shukuno H 2009. Metal-saturated peridotite in the mantle wedge inferred from
1127 metal-bearing peridotite xenoliths from Avacha volcano, Kamchatka. *Earth Planet. Sci. Lett.* 284, 352-360.
1128
1129 Jenniskens P., Shaddad M., Numan D., Elsir S., Kadoda A., Zolensky M., Le L., Robinson G. A., Friedrich
1130 J., Rumble D., Steele A., Chesley S., Fitzsimmons A., Duddy S., Hsieh H., Ramsay G., Brown P., Edwards
1131 W., Tagliaferri E., Boslough M., Spalding R., Dantowitz R., Kozubal M., Pravec P., Borovicka J., Charvat
1132 Z., Vaubaillon J., Kuiper J., Albers J., Bishop L., Mancinelli R., Sandford S., Milam S., Nuevo M. and
1133 Worden S. 2009. The impact and recovery of asteroid 2008 TC₃. *Nature* 458:485-488.
1134
1135 Keil K, Berkley J L and Fuchs L H 1982, Suessite, Fe₃Si: a new mineral in the North Haig ureilite. *American*
1136 *Mineralogist* 67, 126-131
1137
1138 Kita N. T., Ikeda Y., Togashi S., Liu Y., Morishita Y. and Weisberg M. K. 2004. Origin of ureilites inferred
1139 from a SIMS oxygen isotopic and trace element study of clasts in the Dar al Gani 319 polymict ureilite.
1140 *Geochimica et Cosmochimica Acta* 68:4213-4235.
1141
1142 Laurretta D S, Buseck P R and Zega T J. 2001. Opaque minerals in the matrix of the Bishunpur (LL3.1)
1143 chondrite: constraints on the chondrule formation environment. *Geochimica et Cosmochimica Acta* 65,
1144 1337-1353.
1145
1146 Li G, Bai W, Shi N, Fang Q, Xiong M, Yang J, Ma Z and Rong H 2002. Linzhiite, FeSi₂, a redefined and
1147 revalidated new mineral species from Luobusha, Tibet, China. *European Journal of Mineralogy*, 24, 1047-
1148 1052
1149
1150 Litasov K D, Kagi H and Bekker T B. 2019. Enigmatic super-reduced phases in corundum from natural
1151 rocks: Possible contamination from artificial abrasive materials or metallurgical slags. *Lithos* 340-341: 181-
1152 190.
1153
1154 Lodders K. 2003. Solar System Abundances and Condensation Temperatures of the Elements. *The*
1155 *Astrophysical Journal* 591, 1220-1247.
1156
1157 McDonough W F 2003, Compositional model of the Earth's core. In: *Treatise on Geochemistry*, volume 2,
1158 547-568.
1159
1160 Mittlefehldt D. W., McCoy T. J., Goodrich C. A., and Kracher A. 1998. Non-chondritic meteorites from
1161 asteroidal bodies, In: *Planetary Materials, editor Papike J. J. Reviews in Mineralogy and Geochemistry* 36.
1162 *Mineralogical Society of America, Washington, DC, pp 4.1-4.195.*
1163
1164 Mittlefehldt D W, Herrin J S, and Downes H 2007. Petrology and geochemistry of new ureilites and ureilite
1165 genesis. 70th Meteoritical Society Meeting, Abstract #5280.
1166
1167 Moggi Cecchi V, Caporali S, and Pratesi G 2015. DaG 1066: A newfound anomalous ureilite with
1168 chondritic inclusions. 78th Annual Meeting of the Meteoritical Society. Abst. # 5252.
1169
1170 Nakamura-Messenger K, Keller L P, Clemett S J, Messenger S R, Jones J H, Palma R L, Pepin R O, Klock
1171 W, Zolensky M E and Tatsuoka H 2010. Brownleeite: a new manganese silicide mineral in an interplanetary
1172 dust particle. *American Mineralogist*, 95 221-228.
1173
1174
1175
1176

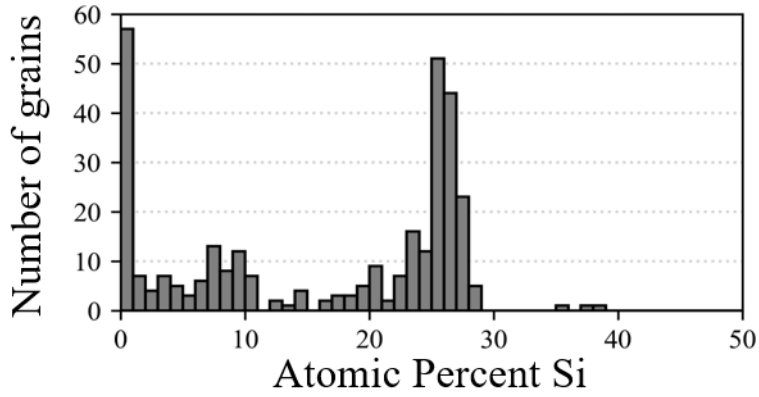
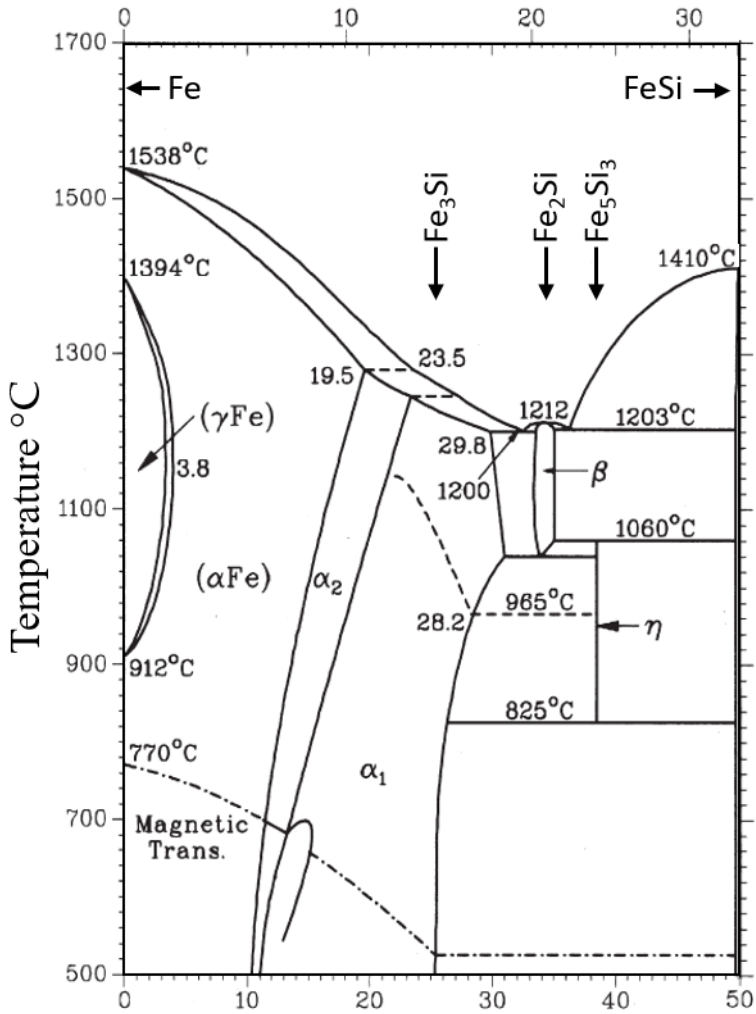
- 1177
1178
1179 Nazarov M A, Demidova S I, Anosova M O, Kositsyn Yu A, Ntaflos Th and Brandstetter F 2012. Native
1180 silicon and iron silicides in the Dhofar 280 lunar meteorite. *Petrology* 20, 506-519.
1181
- 1182 Ott U., Löhr H. P., and Bergemann F. 1990. EET 83309: a ureilite with solar noble gases. *Meteoritics* 25,
1183 396 (Abstract)
1184
- 1185 Ott U., Löhr H. P., and Bergemann F. 1993. Solar noble gases in polymict ureilites and an update on ureilite
1186 noble gas data. *Meteoritics* 28:415-416.
1187
- 1188 Pankov VYu and Spetsius Z V 1989. Inclusions of iron silicides and native silicon in moissanite from the
1189 Sytykanskaya kimberlite pipe. *Doklady Acad, Nauk. SSSR* 305, 152-155 (in Russian)
- 1190 Parnell J, Thackrey S, Muirhead D, and Wright A 2008. Transient high-temperature processing of silicates
1191 in fulgurites as analogues for meteorite and impact melts. 39th LPSC, Abstract # 1286.
1192
- 1193 Pasek M. A. and Pasek V. D. 2018. The forensics of fulgurite formation. *Mineralogy Petrology* 112, 185–
1194 198. <https://doi.org/10.1007/s00710-017-0527-x>.
1195
- 1196 Pasek M A, Block K and Pasek V 2012. Fulgurite morphology: a classification scheme and clues to
1197 formation. *Contrib. Mineral. Petrol* 164, 477-492.
1198
- 1199 Prinz M., Weisberg M. K., Nehru C. E., and Delaney J. S. 1987. EET 83309, a polymict ureilite: recognition
1200 of a new group. *Lunar and Planetary Science* 18:802–803.
- 1201 Rai V. K., Murthy A. V. S. and Ott U. 2003. Noble gases in ureilites: cosmogenic, radiogenic and trapped
1202 components. *Geochimica et Cosmochimica Acta* 67:4435–4456.
1203
- 1204 Rankenburg K., Humayun M., Brandon A. D., and Herrin J. S. 2008. Highly siderophile elements in
1205 ureilites. *Geochimica et Cosmochimica Acta* 72:4642-4659.
1206
- 1207 Reitmeijer F J M, Nakamura T, Tsuchiyama A, Uesugi K, Nakano T and Leroux H 2008. Origin and
1208 formation of iron silicide phases in the aerogel of the Stardust mission. *Meteoritics and Planetary Science*
1209 43, 121-134.
- 1210 Ross A J, Downes H, Smith C L and Jones A P 2009. Highly reduced metals and sulfides in ureilites:
1211 remnants of the UPB core? *Meteoritics and Planetary Science* 44, #5269 (Abst).
1212
- 1213 Ross A J, Downes H, Smith C L and Jones A P. 2010. DaG 1047: a polymict ureilite containing exotic
1214 clasts including a chondrite. 41st LPSC Abstract #2361.
1215
- 1216 Russell S S, Zipfel J, Grossman J N and Grady M M 2002. The Meteoritical Bulletin 86, 2002 July.
1217 *Meteoritics and Planetary Science* 37, Supplement A157-A184
1218
- 1219 Russell S S, Zipfel J, Falco L, Jones R, Grady M M, McCoy T and Grossman J N 2003. The Meteoritical
1220 Bulletin 87. *Meteoritics and Planetary Science* 38, Supplement A189-A248.
1221
- 1222 Schmitt W, Palme H and Wänke H 1989. Experimental determination of metal/silicate partition
1223 coefficients for P, Co, Ni, Cu, Ga, Ge, Mo, and W and some implications for the early evolution of the
1224 Earth. *Geochimica et Cosmochimica Acta* 53, 173-185
1225
- 1226 Scott E. R. D., Taylor J. G., and Keil K. 1993. Origin of ureilite meteorites and implications for planetary
1227 accretion. *Geophysical Research Letters* 20:415-418.
1228

- 1233
1234
1235 Shi N, Bai W, Li G, Xiong M, Yang J, Ma Z, Rong H 2012. Naquite, FeSi, a new mineral species from
1236 Luibusha, Tibet, Western China. *Acta Geologica Sinica* 86, 533-538.
1237
1238 Shiryayev A A, Griffin W L, Stoyanov E and Kagi H 2008. Natural silicon carbide from different geological
1239 settings: polytypes, trace elements, inclusions. 9th Int. Kimb. Conf. Extended Abst. 9IKC-A-00075.
1240
1241 Singletary S. J. and Grove T. L. 2003. Early petrogenetic processes on the ureilite parent body. *Meteoritics*
1242 *and Planetary Science* 38:95-108.
1243
1244 Singletary S. J. and Grove T. L. 2006. Experimental constraints on ureilite petrogenesis. *Geochimica et*
1245 *Cosmochimica Acta* 70, 1291-1308
1246
1247 Smith C L, Wright I P, Franchi I A and Grady M M 2000. A statistical analysis of mineralogical data from
1248 Frontier Mountains ureilites. *Meteoritics and Planetary Science* 35, #5, Supplement p A150.
1249
1250 Smith C L, Downes H, and Jones A P 2008. Metal and sulphide phases in interstitial veins in “dimict”
1251 ureilites – insights into the history and petrogenesis of the Ureilite Parent Body. 39th LPSC Abstract # 1669.
1252
1253 Smith C L, Ross A J, and Downes H 2010. Iron silicide in polymict ureilites – recording the complex history
1254 of the ureilite parent body. Abstract # 5221, 73rd Meeting of Meteoritical Society.
1255
1256 Suttle M D and Genge M J 2017. Diagenetically altered fossil micrometeorites suggest cosmic dust is
1257 common in the geological record. *Earth Planet. Sci. Lett.* 476, 132-142.
1258
1259 van Kooten E.M.M.E., Schiller M. and Bizzarro M. 2017. Magnesium and chromium isotope evidence for
1260 initial melting by radioactive decay of ²⁶Al and late stage impact-melting of the ureilite parent body.
1261 *Geochimica et Cosmochimica Acta* 208, 1-23.
1262
1263 Viswanathan A, Sastikumar D, Kumar H and Nath A K., 2009. Formation of WC-iron silicide (Fe₅Si₃)
1264 composite clad layer on AISI 316L stainless steel by high power (CO₂) laser. *Surface and Coatings*
1265 *Technology* 203, 1618-1623.
1266
1267 Warren P.H. 2012. Parent body depth–pressure–temperature relationships and the style of the ureilite
1268 anatexis. *Meteoritics & Planetary Science* 47, 209-227.
1269
1270 Warren P. H. and Kallemeyn G. W. 1989. Geochemistry of polymict ureilite EET 83309, and a partially
1271 disruptive impact model for ureilite origin. *Meteoritics* 24:233-246.
1272
1273 Warren P. H. and Kallemeyn G. W. 1992. Explosive volcanism and the graphite-oxygen fugacity buffer on
1274 the parent asteroid(s) of the ureilite meteorites. *Icarus* 100:110-126.
1275
1276 Warren P. H. and Huber H. 2006. Ureilite petrogenesis: A limited role for smelting during anatexis and
1277 catastrophic disruption. *Meteoritics and Planetary Science* 41:835-849.
1278
1279 Warren P H, Ullf-Moller F, Huber 2006. H and Kallemeyn G W 2006. Siderophile geochemistry of
1280 ureilites: a record of early stages of planetesimal core formation. *Geochimica et Cosmochimica Acta* 70,
1281 2104-2126
1282
1283 Warren P H and Rubin A E. 2010. Pyroxene-selective impact smelting in ureilites. *Geochimica et*
1284 *Cosmochimica Acta* 74, 5109-5133.
1285
1286 Wasson J T and Wai C M 1970. Composition of the metal, schreibersite and perryite of enstatite achondrites
1287 and the origin of enstatite chondrites and achondrites. *Geochimica et Cosmochimica Acta* 34, 169-184
1288

- 1289
1290
1291 Wasson J T, Ouyang X, Wang J, and Jerde E. 1989. Chemical classification of iron meteorites: XI. Multi-
1292 element studies of 38 new irons and the high abundance of ungrouped irons from Antarctica. *Geochimica*
1293 *et Cosmochimica Acta* 53, 735-744.
1294
1295 Wasson J, Choi B-G, Jerde E, Ulff-Møller F. 1998. Chemical Classification of Iron Meteorites: XII. New
1296 Members of the Magmatic Groups. *Geochimica et Cosmochimica Acta*: 62, 715-724.
1297
1298 Wu Y, Sharma M, LeCompte M A, Vemiroff M N, and Landis J D 2013. Origin and provenance of
1299 spherules and magnetic grains at the Younger Dryas boundary. *Proc. Nat. Acad. Sci.*, 110, 3557-3566.
1300
1301 Yang C.-W., Williams D. B. and Goldstein J. I. 1996. A revision of the Fe-Ni phase diagram at low
1302 temperatures (<400 °C). *Journal of Phase Equilibria* 17, 522-531.
1303
1304 Ye Z, Gupta S, Kerckonen O, Kanniala R, and Sahajwalla V., 2013. SiC and ferro-silicides formation in
1305 Tuyere cokes. *Iron and Steel Institute of Japan International* 53, 181-183.
1306
1307 Yu Z 1984. Two new minerals gupeite and xifengite in cosmic dusts from Yanshan. *Acta Petrologica*
1308 *Mineralogica et Analytica*. 3, 231-238.
1309
1310 Yuan W J, Li R, Shen Q and Zhang L M., 2007. Characterization of the evaluation of the solid solubility
1311 of Si in sintered Fe-Si alloys using DSC technique. *Materials Characterization* 58, 376-379
1312
1313 Yusupov R G, Stanley C J, Welch M D, Spratt J, Cressey G, Rumsey M S, Seltmann R and Igamberdiev E
1314 2009. Mavlyanovite, Mn₅Si₃: a new mineral species from a lamproite diatreme, Chatkal Ridge, Uzbekistan.
Mineralogical Magazine 73, 43-50
1315
1316 Zhang Y, Benoit P and Sears D W 1995. The classification and complex thermal history of the enstatite
1317 chondrites. *Journal of Geophysical Research: Planets*, 100, 9417-9438.
1318
1319 Zolensky M. E., Herrin J. S., Mikouchi T., Ohsumi K., Friedrich J., Steele A., Fries M., Sanford S., Hagiya
1320 K., Takeda H., Colbert M., Hanna R., Maisano J., Ketcham R., Le L., Robinson G.-A., Jenniskens P., and
1321 Shaddad M. H. 2010. Mineralogy and Petrography of the Almahata Sitta Ureilite. *Meteoritics and Planetary*
1322 *Science*. 45, 1618-1637.
1323
1324
1325
1326
1327
1328
1329
1330
1331
1332
1333
1334
1335
1336
1337
1338
1339
1340
1341
1342
1343
1344

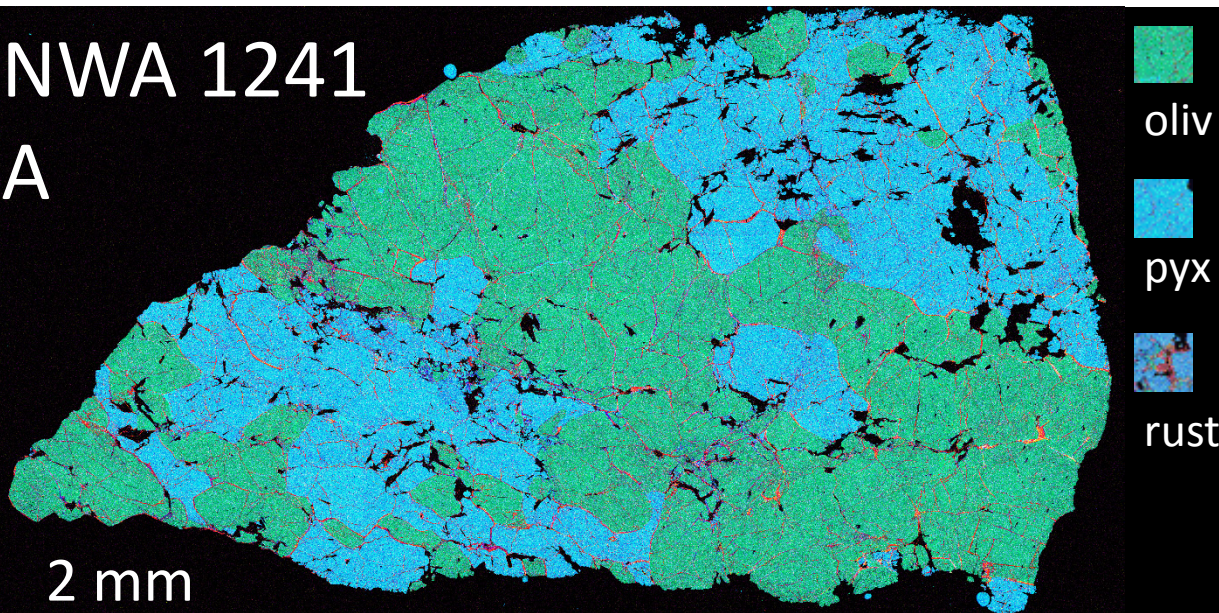


Weight Percent Si

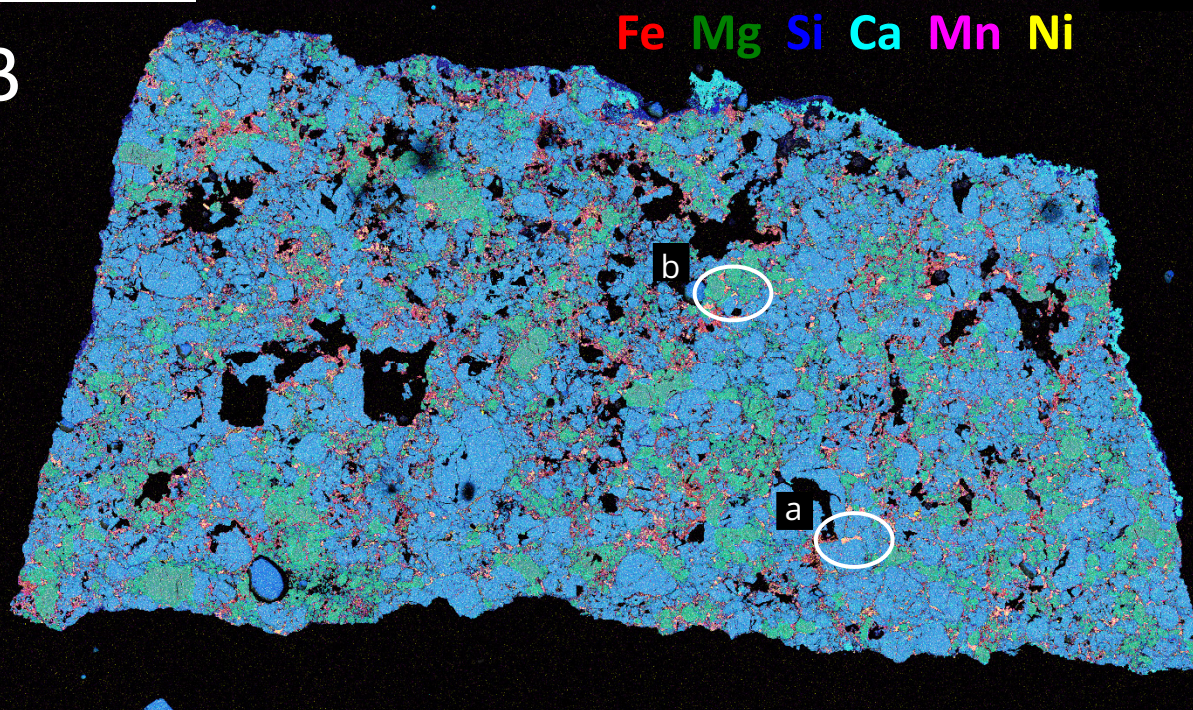


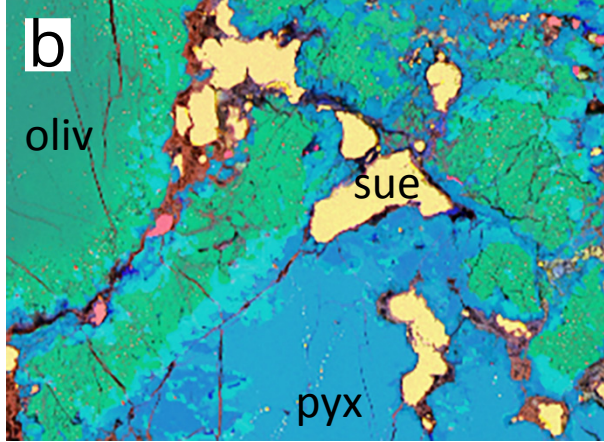
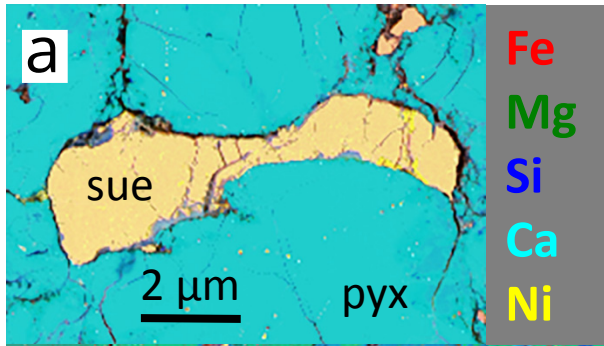
NWA 1241

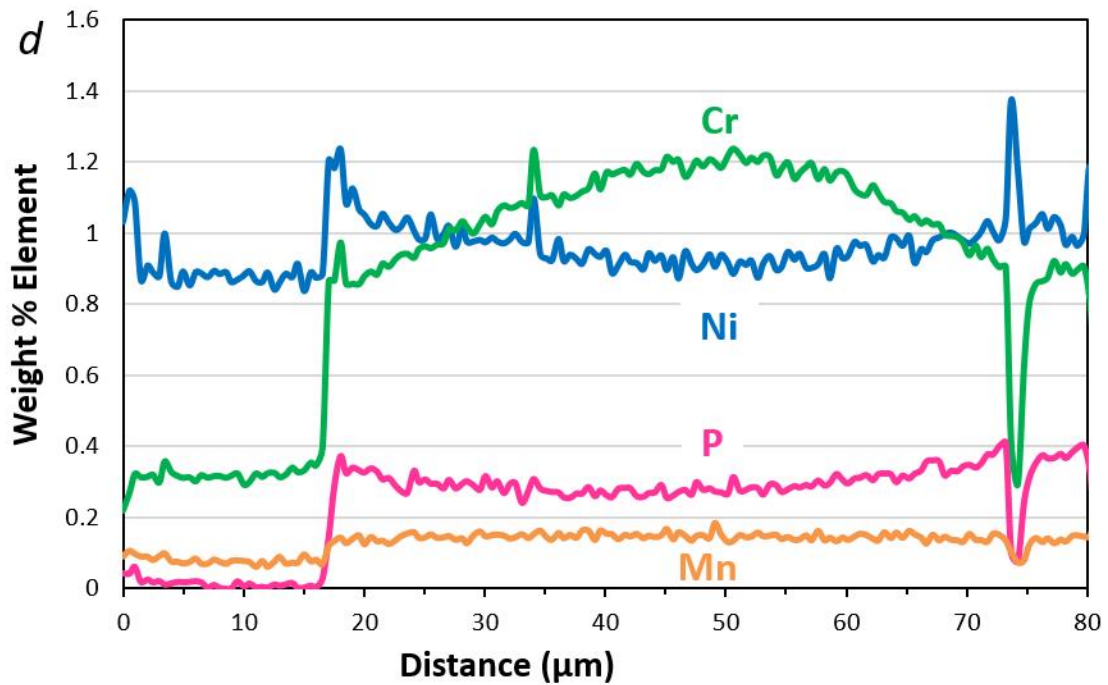
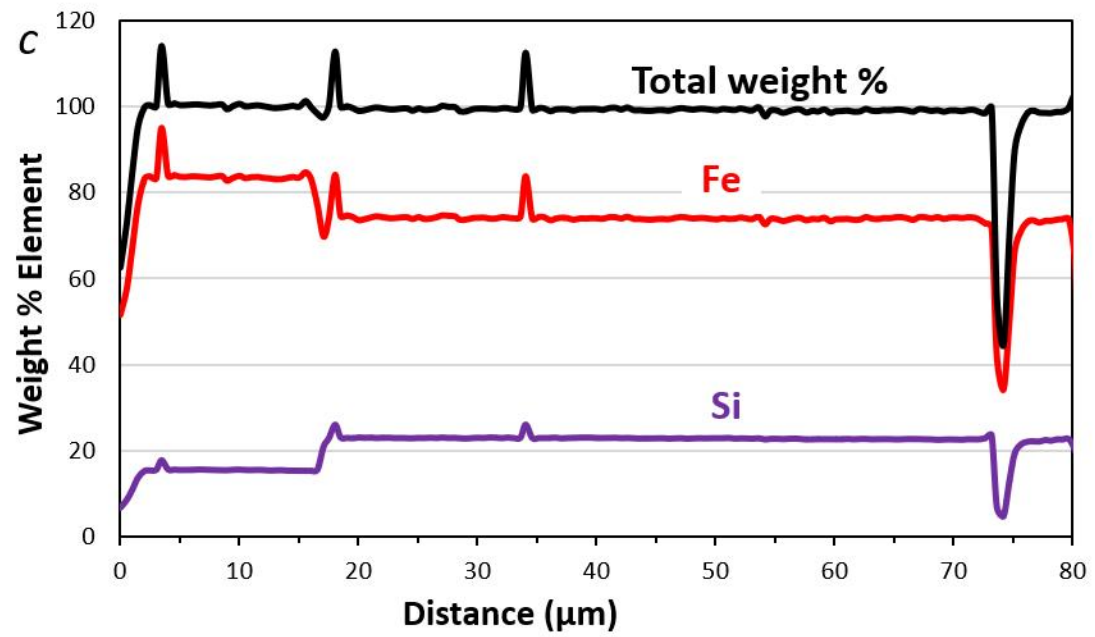
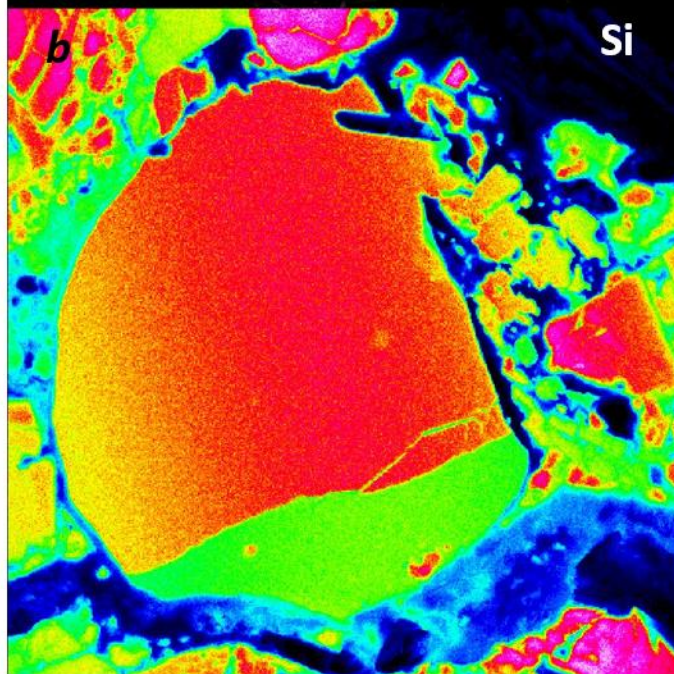
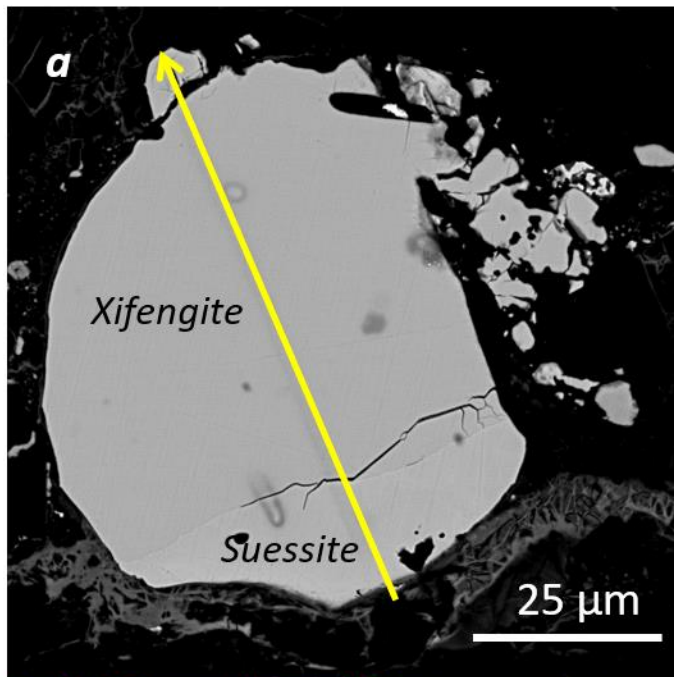
A

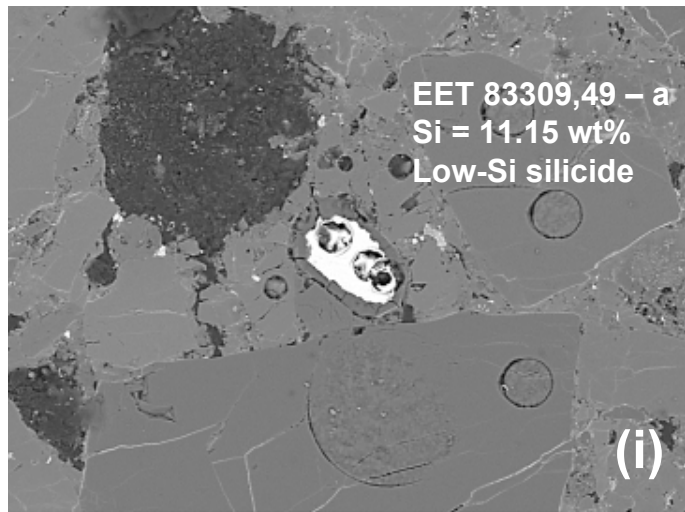


B

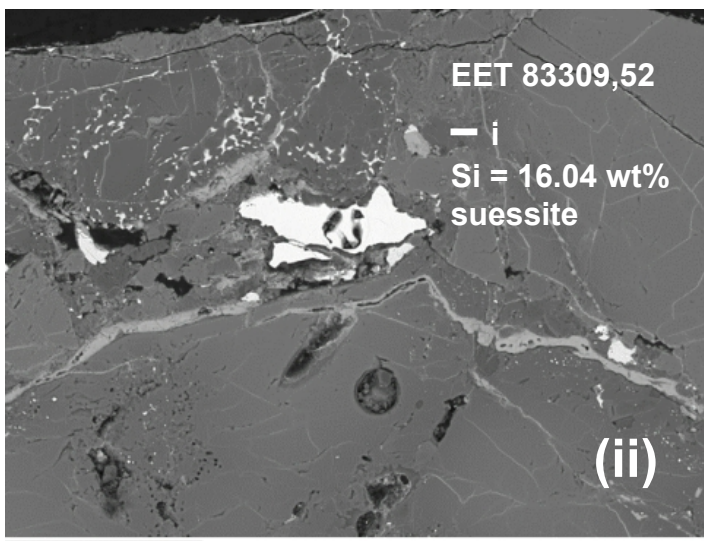




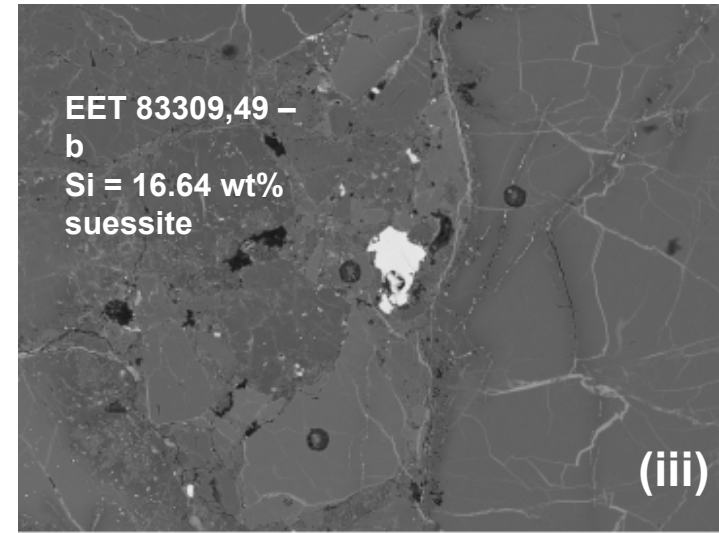




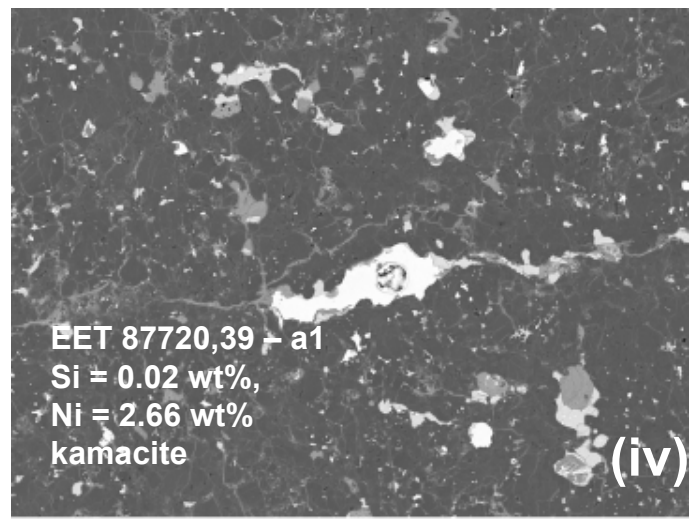
200µm



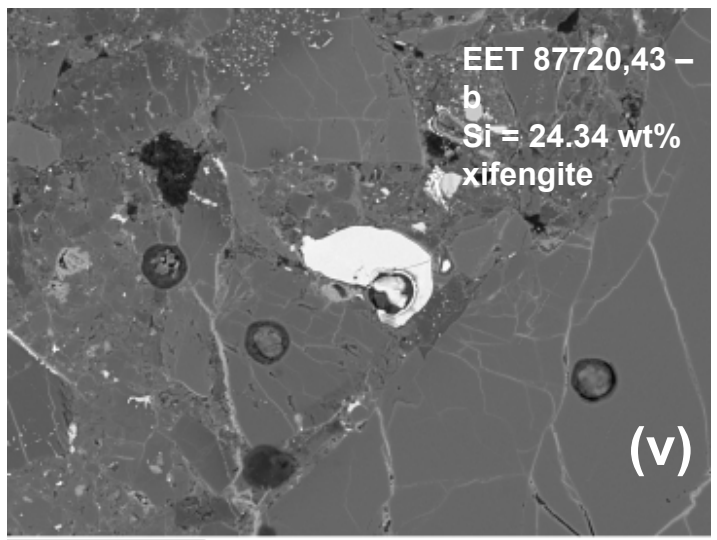
100µm



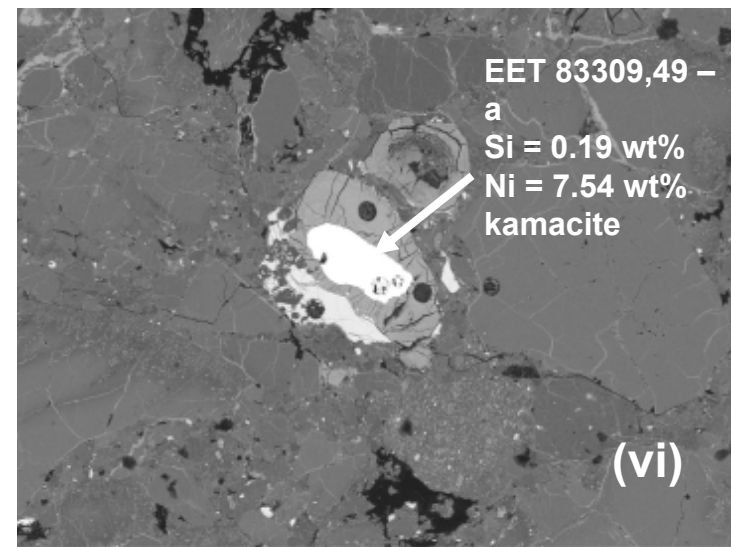
300µm



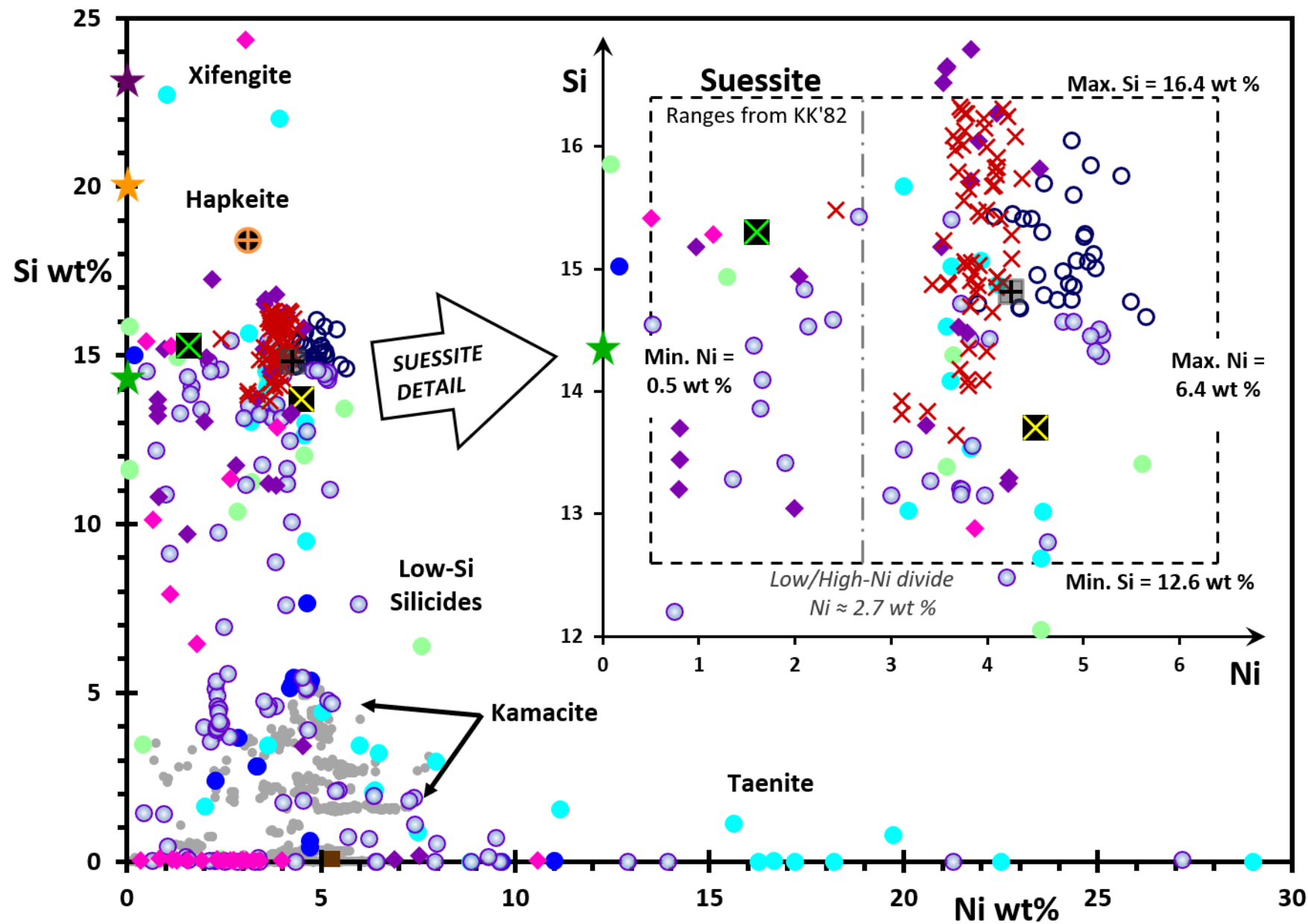
200µm



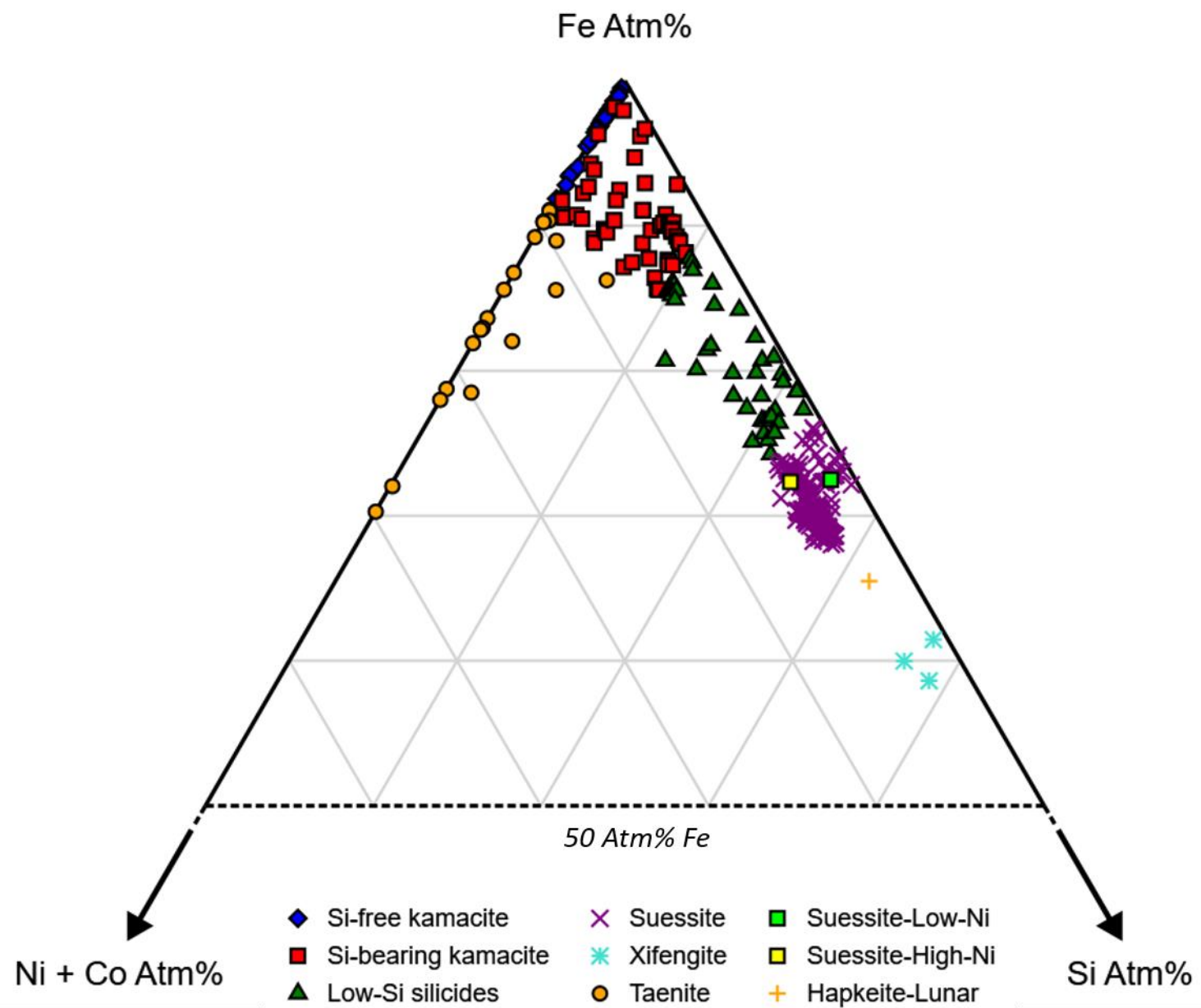
100µm

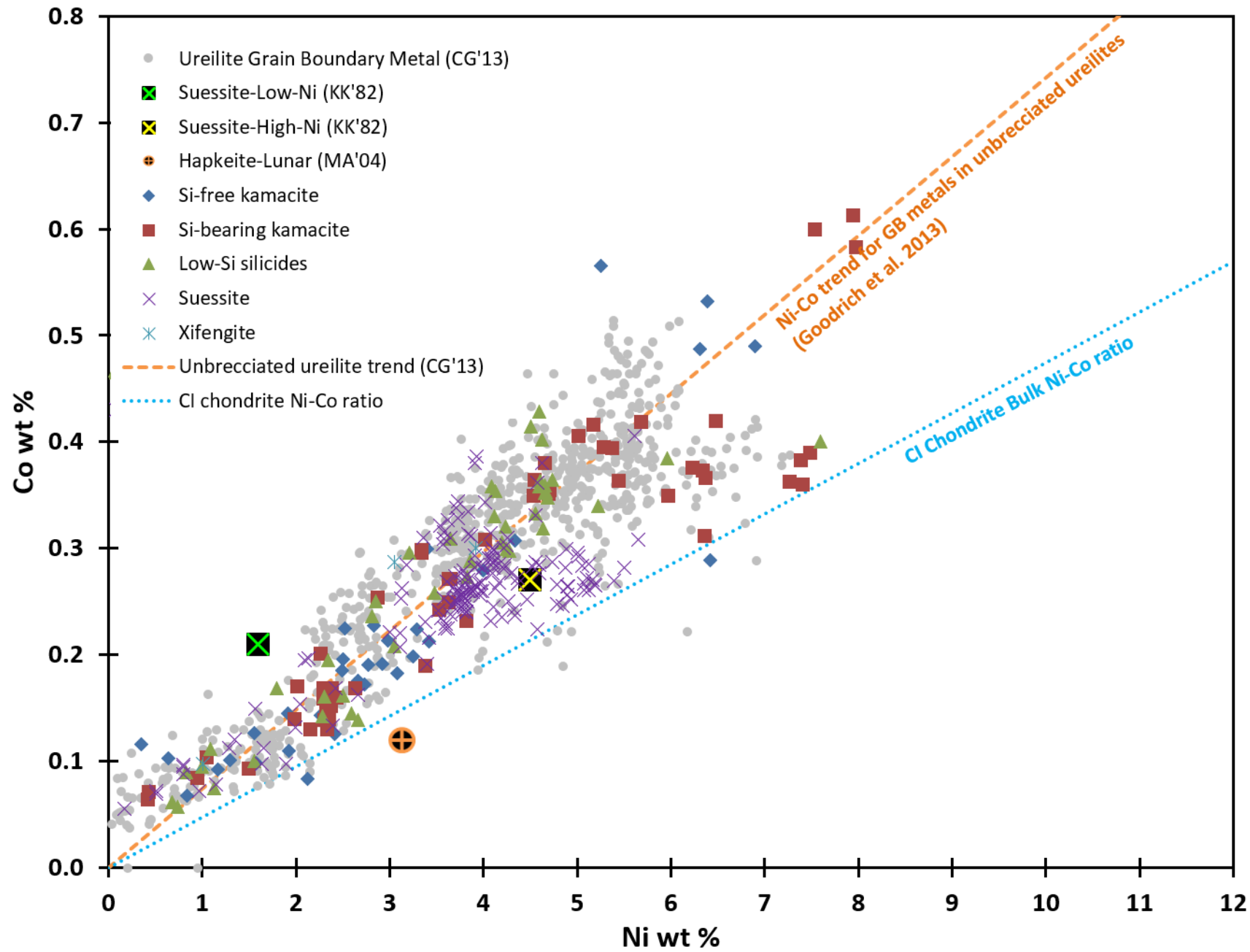


700µm



- DaG 319
- DaG 999
- DaG 1000
- DaG 1023
- DaG 1047
- ◆ EET 83309
- ◆ EET 87720
- NWA 1241-A
- × NWA 1241-B
- Suessite, Low-Ni-KK'82
- Suessite, High-Ni-KK'82
- Suessite-YI'07
- ⊕ Hapkeite, Lunar-MA'04
- ★ Gupeite-Ideal [Fe₃Si]
- ★ Hapkeite-Ideal [Fe₂Si]
- ★ Xifengite-Ideal [Fe₅Si₃]
- Literature GB Metal





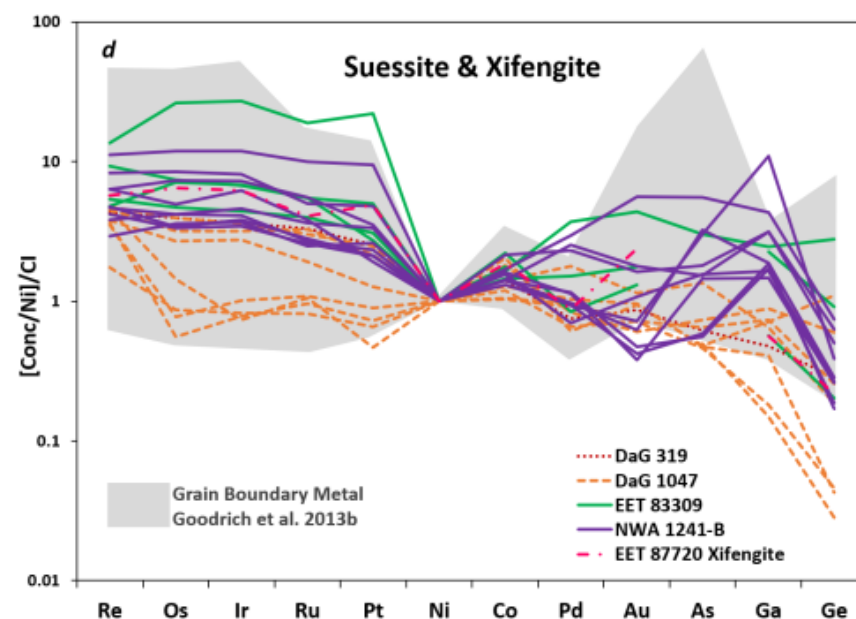
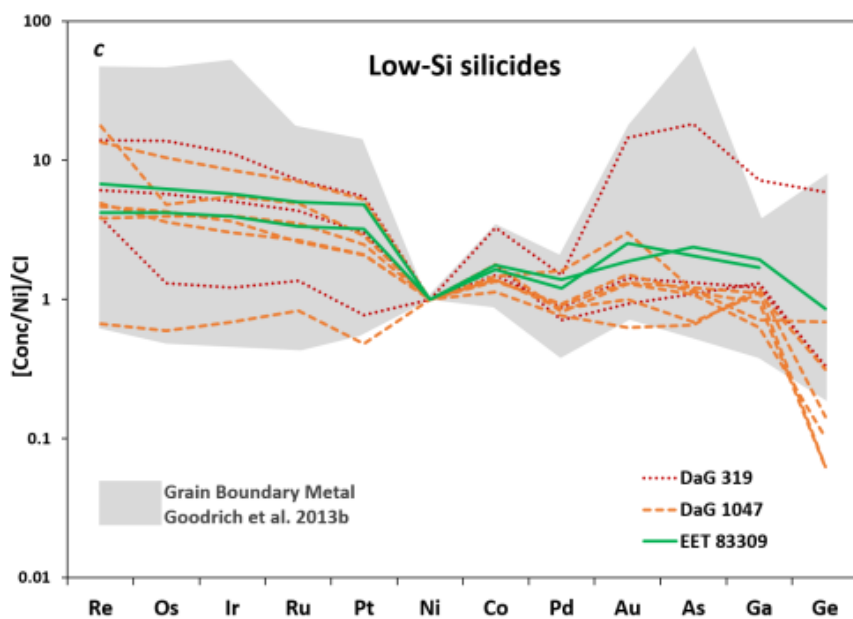
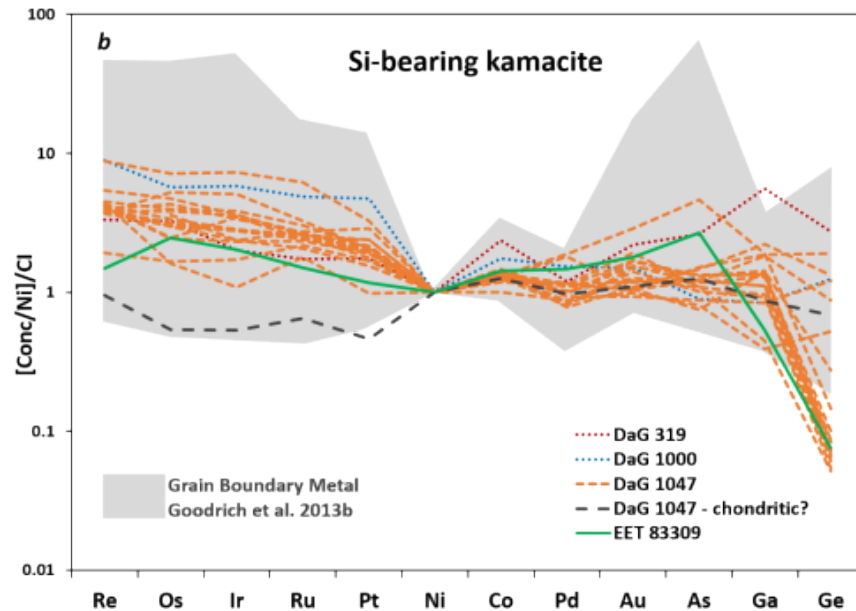
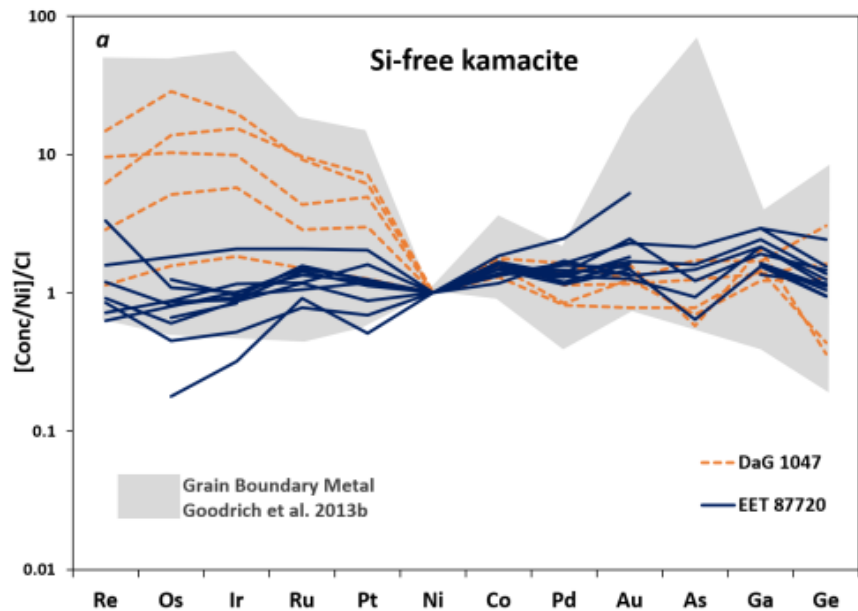


Table 1. Representative major element compositions of metals in brecciated ureilites and NWA 1241-B.

SAMPLE	Si wt%	P wt%	Cr wt%	Mn wt%	Fe wt %	Co wt%	Ni wt%	S wt%	Total wt%
<i>Si-free kamacite</i>									
EET 87720	0.03	0.15	0.06	na	98.02	0.12	0.34	bdl	98.72
EET 87720	0.03	0.17	0.05	na	97.23	0.15	1.92	bdl	99.54
DaG 1000	bdl	0.11	0.09	bdl	95.94	0.14	2.26	bdl	98.55
DaG 319	0.06	0.07	0.10	bdl	96.83	0.13	2.41	bdl	99.59
EET 87720	0.03	0.20	0.12	na	96.33	0.19	2.49	bdl	99.35
DaG 1047	bdl	0.29	0.12	bdl	96.42	0.22	2.52	bdl	99.57
EET 87720	bdl	0.19	0.06	na	96.34	0.21	2.98	bdl	99.78
DaG 1047	bdl	0.06	0.04	bdl	96.77	0.22	3.29	bdl	100.38
DaG 1047	bdl	0.40	0.05	bdl	93.67	0.31	4.34	bdl	98.77
DaG 999	bdl	bdl	bdl	bdl	92.81	0.49	6.31	bdl	99.61
DaG 1047	bdl	0.04	0.07	bdl	93.12	0.53	6.39	bdl	100.14
EET 83309	0.05	bdl	0.05	na	91.87	0.49	6.89	bdl	99.36
<i>Si-bearing kamacite</i>									
EET 83309	0.19	0.45	bdl	na	90.11	7.54	0.60	bdl	98.89
DaG 1047	0.47	0.36	0.07	bdl	96.93	1.05	0.10	bdl	98.98
DaG 1047	0.75	0.56	0.04	bdl	92.24	5.68	0.42	bdl	99.69
DaG 999	0.87	0.15	bdl	bdl	90.35	7.49	0.39	bdl	99.25
DaG 1047	1.44	0.28	0.16	bdl	96.85	0.42	0.06	bdl	99.21
DaG 1047	1.76	0.32	0.06	bdl	93.41	4.02	0.31	bdl	99.88
DaG 1047	1.82	0.37	0.21	bdl	92.08	4.54	0.35	bdl	99.37
DaG 999	2.07	0.06	bdl	0.04	90.94	6.33	0.37	bdl	99.82
DaG 1047	2.14	0.20	0.07	bdl	91.51	5.44	0.36	bdl	99.73
DaG 1000	2.42	0.28	0.39	na	94.02	2.26	0.20	bdl	99.56
DaG 1000	2.83	0.41	0.53	na	92.69	3.34	0.30	bdl	100.10
EET 83309	3.44	0.26	0.06	na	91.04	4.54	0.36	bdl	99.71
DaG 999	3.47	0.33	0.12	0.04	92.07	3.63	0.25	bdl	99.91
DaG 319	3.47	0.08	0.38	bdl	95.73	0.43	0.07	bdl	100.16
DaG 1000	3.69	0.32	0.25	na	92.66	2.87	0.25	bdl	100.04
DaG 1047	3.95	0.47	0.71	bdl	92.39	2.33	0.15	bdl	99.99
DaG 1047	4.11	0.98	0.82	bdl	91.40	2.43	0.16	bdl	99.90
DaG 999	4.44	0.35	0.08	na	88.93	5.01	0.41	bdl	99.21
DaG 1047	4.60	0.42	0.75	bdl	91.77	2.33	0.13	bdl	100.00
DaG 1047	4.91	0.84	0.74	bdl	90.19	2.31	0.16	bdl	99.14
<i>Taenite</i>									
DaG 1000	bdl	0.06	bdl	na	89.19	0.46	9.65	bdl	99.36
EET 87720	bdl	bdl	bdl	na	87.78	0.54	10.58	bdl	98.91
DaG 1047	bdl	0.18	bdl	bdl	85.18	0.77	12.90	bdl	99.01
DaG 999	1.13	0.59	bdl	bdl	81.36	0.76	15.61	bdl	99.45
DaG 999	bdl	bdl	bdl	bdl	81.28	0.70	18.19	bdl	100.17
DaG 1047	bdl	0.66	0.03	bdl	77.47	0.73	21.26	bdl	100.15
DaG 999	bdl	bdl	bdl	bdl	76.58	0.22	22.49	bdl	99.29
DaG 999	bdl	bdl	0.04	na	68.21	1.32	28.99	bdl	98.57

bdl = below detection limit; na = not analysed.

Table 2. Representative major element compositions of silicides in brecciated ureilites and NWA 1241-B.

SAMPLE	Si wt%	P wt%	Cr wt%	Mn wt%	Fe wt %	Co wt%	Ni wt%	S wt%	Total wt%
<i>Low-Si silicides</i>									
DaG 1000	5.26	0.34	0.04	<i>na</i>	89.29	0.35	4.65	<i>bdl</i>	99.94
DaG 1000	5.45	0.24	0.07	<i>na</i>	89.86	0.30	4.27	<i>bdl</i>	100.19
DaG 319	6.38	0.24	<i>bdl</i>	<i>bdl</i>	84.85	0.40	7.60	<i>bdl</i>	99.50
EET 87720	6.46	0.46	0.72	<i>na</i>	90.48	0.17	1.79	<i>bdl</i>	100.09
DaG 1047	6.97	0.04	0.15	<i>bdl</i>	89.59	0.16	2.50	<i>bdl</i>	99.41
DaG 1047	7.64	0.26	0.06	<i>bdl</i>	85.41	0.38	5.96	<i>bdl</i>	99.71
DaG 1047	8.88	0.37	0.40	<i>bdl</i>	85.38	0.27	3.83	<i>bdl</i>	99.14
DaG 999	9.49	0.34	0.13	<i>bdl</i>	85.22	0.43	4.59	<i>bdl</i>	100.20
EET 83309	9.71	0.29	1.11	<i>na</i>	87.40	0.10	1.56	<i>bdl</i>	100.16
DaG 1047	9.77	0.40	0.37	<i>bdl</i>	86.55	0.20	2.35	<i>bdl</i>	99.63
EET 87720	10.13	0.12	0.46	<i>na</i>	88.49	0.06	0.68	<i>bdl</i>	99.95
EET 83309	10.82	0.24	0.30	<i>na</i>	88.08	0.09	0.83	<i>bdl</i>	100.35
DaG 1047	10.90	0.15	0.65	<i>bdl</i>	86.63	0.10	1.00	<i>bdl</i>	99.43
EET 87720	11.34	0.10	0.52	<i>na</i>	85.66	0.14	2.66	<i>bdl</i>	100.42
DaG 319	11.64	0.31	0.66	0.04	86.67	0.47	0.07	<i>bdl</i>	99.83
DaG 1047	11.77	0.21	0.29	<i>bdl</i>	84.01	0.26	3.48	<i>bdl</i>	100.02
<i>Suessite</i>									
DaG 999	12.64	0.10	0.19	<i>bdl</i>	82.69	0.33	4.56	<i>bdl</i>	100.50
DaG 1047	12.77	0.21	0.13	<i>bdl</i>	82.09	0.38	4.63	<i>bdl</i>	100.21
EET 87720	12.88	0.17	0.25	<i>na</i>	82.92	0.31	3.87	<i>bdl</i>	100.41
DaG 999	13.03	0.11	1.41	0.05	81.75	0.28	3.18	<i>bdl</i>	99.80
DaG 1047	13.17	0.10	0.77	<i>bdl</i>	81.93	0.33	3.73	<i>bdl</i>	100.01
EET 83309	13.20	0.05	0.63	<i>na</i>	86.08	0.09	0.79	<i>bdl</i>	100.85
DaG 1047	13.21	0.08	0.76	<i>bdl</i>	82.15	0.34	3.71	<i>bdl</i>	100.24
DaG 319	13.39	0.10	0.39	<i>bdl</i>	82.35	0.25	3.58	<i>bdl</i>	100.06
DaG 1047	13.42	0.09	0.35	<i>bdl</i>	84.29	0.10	1.89	<i>bdl</i>	100.14
EET 83309	13.72	0.08	0.48	<i>na</i>	81.49	0.31	3.36	<i>bdl</i>	99.44
DaG 319	14.30	0.04	0.64	<i>bdl</i>	80.95	0.31	3.65	<i>bdl</i>	99.87
DaG 1047	14.42	<i>bdl</i>	0.36	<i>bdl</i>	80.54	0.28	3.82	<i>bdl</i>	99.42
DaG 1047	14.43	0.07	1.32	0.16	79.04	0.34	4.02	<i>bdl</i>	99.38
DaG 1047	14.46	<i>bdl</i>	0.24	<i>bdl</i>	80.09	0.26	5.08	<i>bdl</i>	100.12
DaG 1047	14.46	0.04	0.24	<i>bdl</i>	80.12	0.27	5.19	<i>bdl</i>	100.32
EET 83309	14.48	0.11	0.09	<i>na</i>	81.92	0.28	3.79	<i>bdl</i>	100.67
DaG 1047	14.51	<i>bdl</i>	0.24	<i>bdl</i>	80.03	0.27	5.17	<i>bdl</i>	100.21
DaG 1047	14.55	<i>bdl</i>	1.23	<i>bdl</i>	82.98	0.07	0.51	<i>bdl</i>	99.34
DaG 1047	14.57	<i>bdl</i>	0.21	<i>bdl</i>	79.83	0.26	4.90	<i>bdl</i>	99.77
DaG 1023	14.61	0.20	0.05	<i>na</i>	79.86	0.31	5.65	<i>bdl</i>	100.68
NWA 1241-B	14.64	0.05	0.59	<i>bdl</i>	80.03	0.29	4.06	<i>bdl</i>	99.66
NWA 1241-B	14.69	0.04	0.76	<i>bdl</i>	80.17	0.26	3.83	<i>bdl</i>	99.75
DaG 1023	14.78	0.19	0.15	<i>na</i>	80.29	0.28	4.60	<i>bdl</i>	100.29
NWA 1241-B	14.81	0.03	0.65	<i>bdl</i>	80.29	0.26	3.89	<i>bdl</i>	99.92
DaG 1047	14.84	<i>bdl</i>	0.83	0.06	82.00	0.20	2.09	<i>bdl</i>	100.01
NWA 1241-B	14.87	0.05	0.69	<i>bdl</i>	80.11	0.26	3.90	<i>bdl</i>	99.89
DaG 1023	14.88	0.22	0.07	<i>na</i>	80.64	0.25	4.85	<i>bdl</i>	100.90
NWA 1241-B	14.89	0.04	0.58	<i>bdl</i>	80.08	0.29	4.16	<i>bdl</i>	100.04
NWA 1241-B	14.91	0.05	0.65	<i>bdl</i>	80.29	0.24	3.82	<i>bdl</i>	99.95
DaG 999	15.02	<i>bdl</i>	1.34	0.05	79.64	0.22	3.62	<i>bdl</i>	99.89
NWA 1241-B	15.03	0.04	0.74	<i>bdl</i>	79.87	0.27	3.91	<i>bdl</i>	99.85
NWA 1241-B	15.03	0.05	0.81	<i>bdl</i>	79.99	0.24	3.78	<i>bdl</i>	99.90
NWA 1241-B	15.05	0.02	0.82	<i>bdl</i>	79.97	0.26	3.84	<i>bdl</i>	99.95

DaG 999	15.07	<i>bdl</i>	0.41	<i>bdl</i>	80.37	0.39	3.93	<i>bdl</i>	100.17
NWA 1241-B	15.08	0.10	0.47	<i>na</i>	80.09	0.30	4.25	<i>bdl</i>	100.29
DaG 1023	15.12	0.08	0.17	<i>na</i>	80.01	0.27	5.10	<i>bdl</i>	100.76
EET 83309	15.18	0.06	0.38	<i>na</i>	80.94	0.24	3.52	<i>bdl</i>	100.32
NWA 1241-B	15.23	0.02	0.95	<i>bdl</i>	79.66	0.23	3.55	<i>bdl</i>	99.64
EET 87720	15.28	0.04	0.39	<i>na</i>	84.48	0.08	1.15	<i>bdl</i>	101.41
DaG 1047	15.43	<i>bdl</i>	1.46	<i>bdl</i>	80.06	0.16	2.66	<i>bdl</i>	99.77
NWA 1241-B	15.46	0.07	0.58	<i>na</i>	79.94	0.28	3.90	<i>bdl</i>	100.24
NWA 1241-B	15.48	0.08	0.69	<i>na</i>	81.81	0.17	2.42	<i>bdl</i>	100.65
NWA 1241-B	15.56	0.08	0.47	<i>na</i>	79.74	0.28	3.76	<i>bdl</i>	99.88
DaG 1023	15.61	0.07	0.28	<i>na</i>	79.58	0.26	4.90	<i>bdl</i>	100.70
DaG 999	15.68	<i>bdl</i>	1.09	0.04	80.14	0.25	3.12	<i>bdl</i>	100.33
DaG 1023	15.70	0.08	0.19	<i>na</i>	79.28	0.28	4.59	<i>bdl</i>	100.12
EET 83309	15.82	0.14	0.58	<i>na</i>	77.71	0.29	4.55	<i>bdl</i>	99.08
DaG 319	15.85	0.34	0.62	<i>bdl</i>	82.88	0.43	0.08	<i>bdl</i>	100.20
NWA 1241-B	16.00	0.06	0.67	<i>na</i>	79.31	0.28	3.99	<i>bdl</i>	100.30
NWA 1241-B	16.08	0.05	0.71	<i>na</i>	79.10	0.28	4.30	<i>bdl</i>	100.51
NWA 1241-B	16.30	<i>bdl</i>	0.73	<i>na</i>	78.92	0.26	3.74	<i>bdl</i>	99.95
NWA 1241-B	16.31	<i>bdl</i>	0.87	<i>na</i>	77.92	0.27	4.17	<i>bdl</i>	99.53
NWA 1241-B	16.32	<i>bdl</i>	0.96	<i>na</i>	79.30	0.25	3.72	<i>bdl</i>	100.55
<i>Xifengite</i>									
DaG 999	22.74	0.28	1.22	0.16	73.77	1.01	0.10	<i>bdl</i>	99.27
DaG 999	22.04	0.81	0.89	<i>na</i>	71.72	3.91	0.30	<i>bdl</i>	99.68

bdl = below detection limit; na = not analysed.